Applied Catalysis A, General 704 (2025) 120410

Contents lists available at ScienceDirect

Applied Catalysis A, General

journal homepage: www.elsevier.com/locate/apcata

Selective photo-oxidation of lignin-based alcohols to aldehydes catalyzed by gold nanoparticles supported on titanate nanotubes and nanowires

Henry Martínez [a,*], Álvaro A. Amaya [b], Fernando Martínez O. [b], Cecilia C. Torres [c], Cristian H. Campos [c,*]

[a] Departamento de Fisicoquímica, Facultad de Ciencias Químicas, Universidad de Concepción, Concepción, Chile
[b] Centro de Investigaciones en Catálisis-CICAT, Universidad Industrial de Santander, Escuela de Química, Km 2 vía El Refugio, Piedecuesta, Santander, Colombia
[c] Departamento de Ciencias Químicas, Facultad de Ciencias Exactas, Universidad Andres Bello, Autopista Concepción-Talcahuano, Talcahuano 7100, Chile

ARTICLE INFO

Keywords:
Lignin-derived alcohols
Selective oxidation
Gold nanoparticles
Hydrogen titanates

ABSTRACT

Photocatalytic conversion of biomass and its derivatives is a promising strategy for producing energy and products of industrial interest. In this study, the selective photooxidation of lignin-derived alcohols (vanillyl and veratryl) to their respective aldehydes was investigated using gold nanoparticles (AuNPs) supported on hydrogen titanate nanotubes (HTNTs) and nanowires (HTNWs) under visible light and O_2 at room temperature and pressure. The results show that the AuNPs/HTNTs and AuNPs/HTNWs systems are highly active and selective in the photooxidation of vanillyl and veratryl alcohol, with conversions above 90 % and selectivity above 95 % toward the formation of vanillin and veratraldehyde, respectively. The preparation of the photocatalytic systems by functionalization with (3-aminopropyl)trimethoxysilane and subsequent deposition–reduction with $NaBH_4$ of Au in successive cycles allowed us to obtain metal loadings of 1, 3 %, and 5 % by mass, controlling the size, dispersion, and stability of the nanoparticles AuNPs. Physicochemical characterization of the solids showed that the incorporation of AuNPs into HTNT and HTNW supports led to an increase in oxygen vacancies, a decrease in the charge transfer resistance of the material, and thus a lower recombination rate of electron–hole pairs. Further studies in the presence of scavenger molecules and electron paramagnetic spectroscopy allowed us to conclude that under visible light, the AuNPs generate photoelectrons that move toward the conduction band of the support, where the reduction of O_2 occurs to form the superoxide radical anion, the main reactive oxygen species causing the oxidation of alcohols.

1. Introduction

Lignocellulosic biomass is a promising carbon source for the sustainable synthesis of fuels and fine chemicals. The three main components of lignocellulosic biomass are hemicellulose, cellulose, and lignin [1]. Lignin produced from wood is an important source of aromatic phenolic compounds such as *p*-coumarylic, *p*-sinapylic, coniferyl, veratryl, and vanillyl alcohols. These industrially interesting lignin-derived model compounds, which contain active functional groups such as phenolic hydroxyl, hydroxymethyl, and methoxyl groups on the benzene ring, can assist in various chemical reactions and synthesis of high-value-added products [2]. Therefore, the oxidation of lignin-based aromatic phenolic compounds to obtain value-added products has attracted considerable research interest [3]. One notable reaction is the selective oxidation of vanillyl alcohol to produce vanillin, which has various applications in food additives, perfumes, pharmaceuticals, and fine chemicals. The most common method to produce vanillin involves stoichiometric reactions between non-renewable fossil fuel-derived compounds such as glyoxalic acid and nitrose [4]. Therefore, it is of interest to develop methods that add value to lignin derivatives.

Usually, the oxidation of the side chains of phenolic compounds requires the use of strong oxidizing agents, such as chromic acid, potassium permanganate, and homogeneous cobalt catalysts. This leads to serious environmental and operational problems, including (i) difficulty in separation from the reaction media, (ii) inability to be reused, and (iii) rapid deactivation due to the formation of μ-oxo dimers [5]. Compared to traditional homogeneous processes with strong oxidants, the design of efficient environmentally friendly heterogeneous catalysts for the oxidation of lignin-based alcohols to aldehydes is highly desirable,

* Corresponding authors.
E-mail addresses: hmartinez@udec.cl (H. Martínez), cristian.campos.f@unab.cl (C.H. Campos).

https://doi.org/10.1016/j.apcata.2025.120410
Received 22 December 2024; Received in revised form 31 May 2025; Accepted 19 June 2025
Available online 20 June 2025
0926-860X/© 2025 Elsevier B.V. All rights are reserved, including those for text and data mining, AI training, and similar technologies.

considering the separation and reusability of the catalysts.

In this vein, the oxidation of lignin-derived alcohols has been reported using noble metal nanoparticles deposited on commercial supports and porous-type materials such as $Ag@SiO_2/CeO_2$ [6], Pd/SiO_2 [7], Pd/C [8], Ru/Al_2O_3 [9], and Ru/TiO_2 [10], among others. Several reports have indicated the advantages of using Au as a co-catalyst in the presence of a suitable support. Vanillin has been selectively obtained by the oxidation of vanillyl alcohol in the presence of Au/ZnO [11], Au/Al_2O_3 [12], Au/CeO_2 [13], and Au/TiO_2 [14] with conversions above 80 % using O_2 as the oxidant. However, in some cases, long reaction times, temperatures above 80 °C, and the addition of NaOH or TEMPO are required to supply the primary hydroxyl groups for preliminary dehydrogenation via proton abstraction. Other non-noble transition metals have also been used in the selective oxidation of vanillyl and veratryl alcohols. Co/ZnO catalysts [13], Co-saponite [5], Co-ZIF-9 [15], Co doping spinel structure $Cu_{0.4}Co_{0.6}Fe_2O_4@PC$ [16], and Fe-Ni/mordenite [17] have been evaluated in the liquid-phase oxidation of vanillyl, veratryl, cinnamyl, and guaiacol alcohol using O_2 as oxidant. In most cases, the reactions are carried out at temperatures above room temperature and high O_2 pressures; in addition to the respective aldehydes, other oxidation products are obtained.

As an alternative route, photocatalysis allows the selective oxidation of alcohols to aldehydes under ambient pressure and temperature. Recently, the heterogeneously catalyzed photooxidation of aromatic alcohols to aldehydes under sunlight and UV–vis light has been extensively studied. Such a strategy can result in relatively short reaction times under mild conditions without the need for additional chemicals. Using air or oxygen as the primary oxidant, the photoproduction of vanillin in an aqueous medium in the presence of TiO_2 powder has been reported [18]. In examples of light-promoted lignin-derived model alcohol oxidation reactions using modified titanium dioxide-based photocatalysts such as W-TiO_2 P25 [19] and $CuBi_2O_4$-TiO_2 (CBO/-TiO_2) [20], functionalization with organic agents or transition metal deposition generates a shift in the absorption edge of the material, facilitating the use of visible light in the photoreactions. One of the most reproducible alternatives for the selective oxidation of alcohols of interest in fine chemistry is sensitization with plasmonic metal nanoparticles (NPs) [21–25]. Previous research has shown that photocatalytic activity in the selective oxidation of alcohols to their corresponding aldehydes is enhanced by the presence of gold nanoparticles (AuNPs) in TiO_2 nanowires [26]. Au is the most studied metal because it has a resonance plasmon that manifests at wavelengths corresponding to the visible light spectrum [27,28].

The size and shape of the NPs, Au atomic coordinative unsaturation, and Au–support interactions are crucial in determining the final performance in oxidative photocatalysis, and these properties in turn depend on the synthesis method [29]. Therefore, it is necessary to develop novel, simple, and efficient preparation methods that allow the preparation of small, uniform AuNPs with strong interactions with the support that are stable and avoid agglomeration. To date, traditional preparation methods, such as chemical adsorption, co-precipitation, deposition–precipitation, chemical vapor deposition, and reverse micelles, have some limitations related to NP size uniformity, Au–support interactions, and complex preparation procedures [11].

Previous studies have reported a simple methodology involving the modification of the TiO_2 support (nanotubes and nanosheets) with 3-aminopropyl-trimethoxysilane (APTMS) to achieve better metal (Au, Pt, Pd) dispersion and its subsequent reduction with $NaBH_4$, having the ability to produce small, highly dispersed, and stable NPs that can be reused in several consecutive reactions [30–32]. Other supports such as hydrogen titanate ($H_2Ti_3O_7$) nanotubes and nanowires (HTNTs and HTNWs, respectively) have also attracted interest due to their mesoporous structure, which provides a high surface area, efficient ion exchange, and a simple preparation method [33]. Additionally, these 1D structures exhibit high surface-to-volume ratios, improved light absorption/scattering, interfacial charge transfer properties, and charge separation efficiencies for enhanced photocatalytic activity [34,35].

In this study, AuNPs supported on HTNTs and HTNWs functionalized with APTMS were prepared, followed by the deposition and reduction of Au for the selective photooxidation of vanillyl and veratryl alcohols to their respective aldehydes. First, the photocatalyst was prepared with a 1 % Au mass loading. The same solid was then subjected to a second deposition–reduction procedure to complete the photocatalyst with 3 % and 5 % Au. A photocatalyst with 5 % Au mass loading was also obtained. The results confirm that this methodology allows small and highly dispersed AuNPs to be obtained and that the interaction with APTMS provides stability to the photocatalytic system. The AuNPs/HTNTs and AuNPs/HTNWs nanocomposites were found to be highly active and selective in the oxidation of lignin-derived alcohols, such as vanillyl and veratryl alcohols, using O_2 and visible light at room temperature.

2. Experimental section

2.1. Materials

All materials were obtained and used without further purification unless otherwise noted. All the solvents were thoroughly degassed before use. Toluene was dried under reflux with metallic sodium. TiO_2 anatase nanopowder < 25 nm particle size 99.7 % trace metal basis, (3-aminopropyl)trimethoxysilane 97 %, tetrachloroauric(III) acid trihydrate 99 % and sodium borohydride 98 %, benzyl alcohol ≥ 99 %, vanillyl alcohol ≥ 98 %, veratryl alcohol 96 %, and myrtenol ≥ 95 % were purchased from Sigma-Aldrich.

2.2. Catalyst preparation

2.2.1. Synthesis of HTNTs and HTNWs

Alkaline high-pressure hydrothermal treatment of TiO_2 anatase nanopowder, followed by ion exchange and calcination, was used to prepare HTNTs and HTNWs [36,37]. Specifically, 1 g of anatase TiO_2 (~25 nm) was dispersed in 40 mL of 10 M KOH solution for HTNWs and 10 M NaOH solution for HTNTs. The resulting suspension was stirred for 30 min to obtain a uniform suspension. The mixture was maintained at 110 °C for HTNTs and 200 °C for HTNWs for 24 h in a 100 mL Teflon-lined autoclave. The resulting solids were washed with 0.1 M HNO_3 solution to a pH of ~1 and with deionized water several times until a pH of ~7 was reached. The resulting powders were collected by centrifugation and dried at 80 °C for 12 h to produce HTNTs and HTNWs.

2.2.2. Preparation of deposited AuNPs

Prior to Au deposition, the supports, HTNTWs and HTNTs, were modified with APTMS using a method reported previously [30,31]. In a round flask, 1 g of each solid compound was added into 50 mL of dry toluene and 100 μL of APTMS and refluxed for 24 h. The solid so obtained was dispersed in distilled water, and then the necessary amount of $HAuCl_4 \bullet 3\ H_2O$ was added to complete 1 % loading. Subsequently, an appropriate amount of freshly prepared $NaBH_4$ solution was added to completely reduce the Au and the mixture was stirred for 45 min, as shown in Fig. 1. The resulting sample was centrifuged, washed several times, and dried at 80 °C. The catalysts with 3 % and 5 % loading were prepared by successive dispersion, i.e., from 1 % catalyst, by adding a sufficient amount of Au to reach a total loading of 3 %. Thereafter, the 5 % Au catalyst was prepared from the catalyst with 3 % Au, following the same dispersion–reduction procedure with $NaBH_4$.

2.3. Catalyst characterization

A Bruker AXS D8 Advance DaVinci geometry instrument with monochromated Cu Kα radiation (λ= 1.5418 Å) at 40 kV and 30 mA was used to determine the X-ray diffraction (XRD) patterns of the TiO_2-based

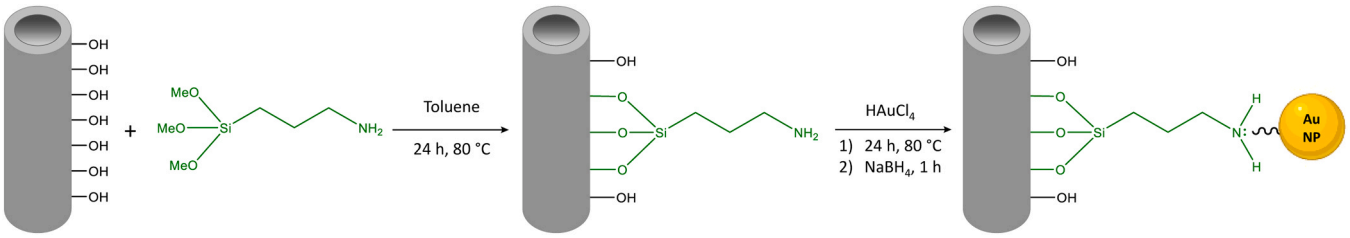


Fig. 1. Process for the preparation of catalysts based on Au NPs deposited on $H_2Ti_3O_7$ nanostructures by functionalization of the support with APTMS.

supports. The diffraction pattern was collected in the 2θ value range of 10°–90° (with a step size of 0.01° and a step time of 0.4 s). The morphologies of the AuNPs and the support were determined by transmission electron microscopy (TEM) using a JEOL model JEM-1200 EXII with ImageJ software. Micromeritics TriStar II 3020 apparatus was used to determine the textural properties of the catalysts by performing N_2 adsorption–desorption isotherms at −196°C. Specific surface areas were determined by the Brunauer–Emmett–Teller (BET) equation using adsorption data over a relative pressure range between 0.05 and 0.3, and pore size distributions were estimated using the Barrett–Joyner–Halenda (BJH) method. The samples were degassed at 120 °C for 3 h prior to determining the surface areas and pore size distributions. A Thermo Scientific (Waltham, MA, USA) Evolution 260 UV–Vis spectrophotometer equipped with a xenon flash lamp and a 60 mm integrating sphere with Spectralon® coating was employed to measure the diffuse reflectance spectra collected in the 200–900 nm spectral range to evaluate the visible light response of AuNPs/$H_2Ti_3O_7$ nanocomposites in powder samples. A Perkin Elmer Elas6000 ICP-MS spectrometer was used for chemical analysis via inductively coupled plasma mass spectrometry. To determine the surface elemental composition of the catalyst, X-ray photoelectron spectroscopy (XPS) was obtained using the SPECS® XPS/ISS/UPS surface characterization platform of the Laboratorio de Ciencia de Superficies of the Universidad Industrial de Santander and analyzed using Casa XPS software. All signals were analyzed using the Shirley background. The Au 4 $f_{7/2}$ and Au 4 $f_{5/2}$ signals of the Au^0 species were fitted to asymmetric line shapes, and the relative sensitivity factors for the Au 4 f and Ti 2p signals were recorded to be 17.92 % and 7.57 %, respectively.

2.4. Photoelectrochemical measurements of the films

Photoelectrochemical (PEC) characterization of the films was performed using the typical three-electrode cell with a potentiostat (AUTOLAB PGSTAT 302 N). A graphite rod (99.9995 % pure, Alfa Aesar) was used as the counter electrode, and an Ag/AgCl (3 M KCl) as the reference electrode. A Pt foil and SCE were used as the counter and reference electrodes, respectively. The frequency range of the electrochemical impedance spectroscopy (EIS) test was set to 100 kHz to 10 mHz with an applied sinusoidal potential amplitude of 5 mV.

2.5. Oxidation reactions of lignin-derived alcohols

The photooxidation reactions of lignin-derived alcohol solutions (0.1 M) were performed in a reactor equipped with a cooling system to maintain a constant temperature. An Osram Powerstar HQI-E 400 W (λ>400 nm), oxygen bubbling, and stirring at 300 rpm were used. The catalyst was added to the reaction medium (maintaining an Au/alcohol molar ratio of 100) and stirred until adsorption equilibrium was reached. The light was then turned on and the reaction was monitored by collecting the samples at intervals of 1 h during the course of the reaction. After the reactions reached completion, the catalyst was immediately separated from the suspension by filtration through a 0.45 μm membrane filter (Merck Millex™-HV, PVDF, 0.45 μm). The solution was then analyzed by gas chromatography using a Shimadzu GC-2030, capillary column: Rtx-5 amine, 30 m, 0.53 mm ID, 3.00 μm. Stability tests were performed up to ten times, separating the catalyst at the end of the reaction, followed by washing and drying before use in the subsequent reactions.

3. Results and Discussion

3.1. Physico-chemical characterization

Fig. 2 shows the X-ray powder diffraction (XRD) patterns of the HTNTs and HTNWs supports and the corresponding Au-modified catalysts. The diffraction peaks of bare HTNTs and HTNWs corresponded to the layered or tunneled titanate structure, $H_2Ti_nO_{2n+1}{\cdot}xH_2O$ (JCPDS#36–0654) [38]. In all Au-modified samples, a decrease in the intensity of the peaks was observed. The decrease in intensity increased with increasing Au content of the supports. For both HTNTs and HTNWs supports, the characteristic signals of the metal were noticeable only at 5 % Au due to Au content in the catalyst. Peaks at 38.2°, 44.3°, and 64.3° corresponded to the [111], [200], and [220] reflections of metallic Au (JCPDS#004–784), respectively [39]. For the catalysts with 1 % and 3 % Au, no characteristic XRD patterns of the AuNPs were detected in the XRD patterns due to the small size of the particles (<4 nm). The reflection peak at 2θ ~ 10° shifted to a higher angle and became broader. This reflection peak was related to the interlayer (or tunnel–tunnel) spacing of titanate. Consequently, the shift in these signals indicated a decrease in the interlayer spacing. This is due to the dehydration of the H_2O molecules contained in the as-synthesized nanowires and nanotubes during Au modification [40,41].

The nanotubes and nanowires were subject to hydrothermal treatment and characterized (see SI, Fig. S1). The morphology of the AuNPs supported on HTNTs and HTNWs was characterized by TEM. It was observed that HTNTs resembled a rolled-up carpet with a length of 50–200 nm, an inner diameter of 4–8 nm, and an outer diameter of 8–15 nm, and consisted of multiple (4–7) walls separated by about 1 nm, which corresponded to the 0.78 nm (100) interplanar distance of $H_2Ti_3O_7$ [42,43]. HTNWs were formed from $H_2Ti_3O_7$ sheets arranged into 50–1000 nm long and 15–50 nm thick structures with an approximately rectangular cross section and no hollow inner channel. As shown in Fig. 3a–c for the HTNTs loaded with 1 %, 3 %, and 5 % by weight of Au and Fig. 3d–f for the HTNWs with the same distribution of Au, the AuNPs had a spherical shape and were homogeneously distributed on the surface of the HTNTs and HTNWs. For both supports, the size of the NPs increased from 2.0 nm for 1 % Au loading, to 4.5 nm for 5 % Au loading. Furthermore, the lattice spacing of 0.23 nm confirmed the formation of the [111] Au crystal plane (inset Fig. 3c,f). These results confirmed that the method of APTMS surface functionalization and subsequent metal loading to obtain the 3 % and 5 % systems is efficient to prepare catalysts with higher metal loading while retaining the small and uniform size of AuNPs with good dispersion. In this case, the smaller NPs act as seeds that allow the metal to be deposited in subsequent reactions and cause the increase in NP size.

Table 1 summarizes the textural properties of the solids. The surface area was determined by the BET method from the N_2 adsorption–desorption isotherms at −196°C. In all cases, the isotherms of the

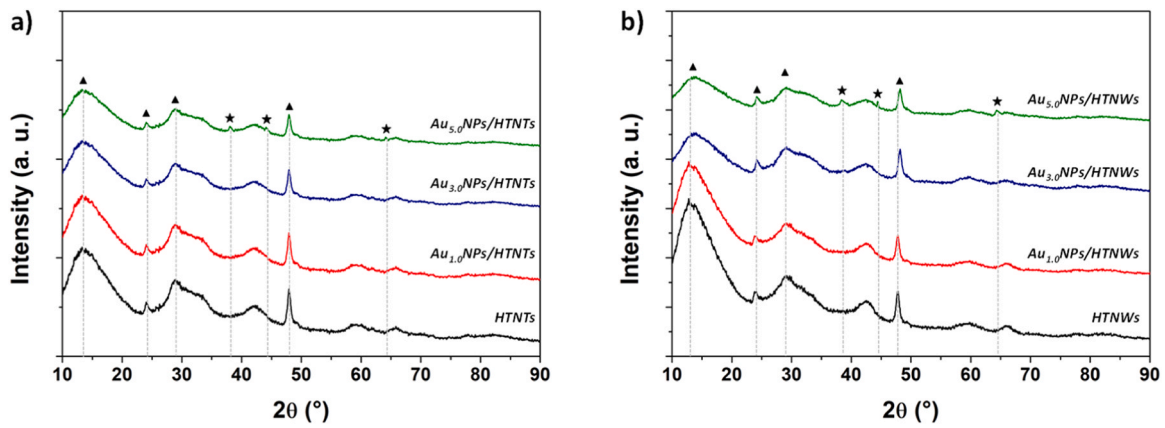


Fig. 2. X-ray diffraction (XRD) patterns of pristine and Au-modified a) HTNTs and b) HTNWs photocatalysts (▲ hydrogen titanate ★ metallic gold).

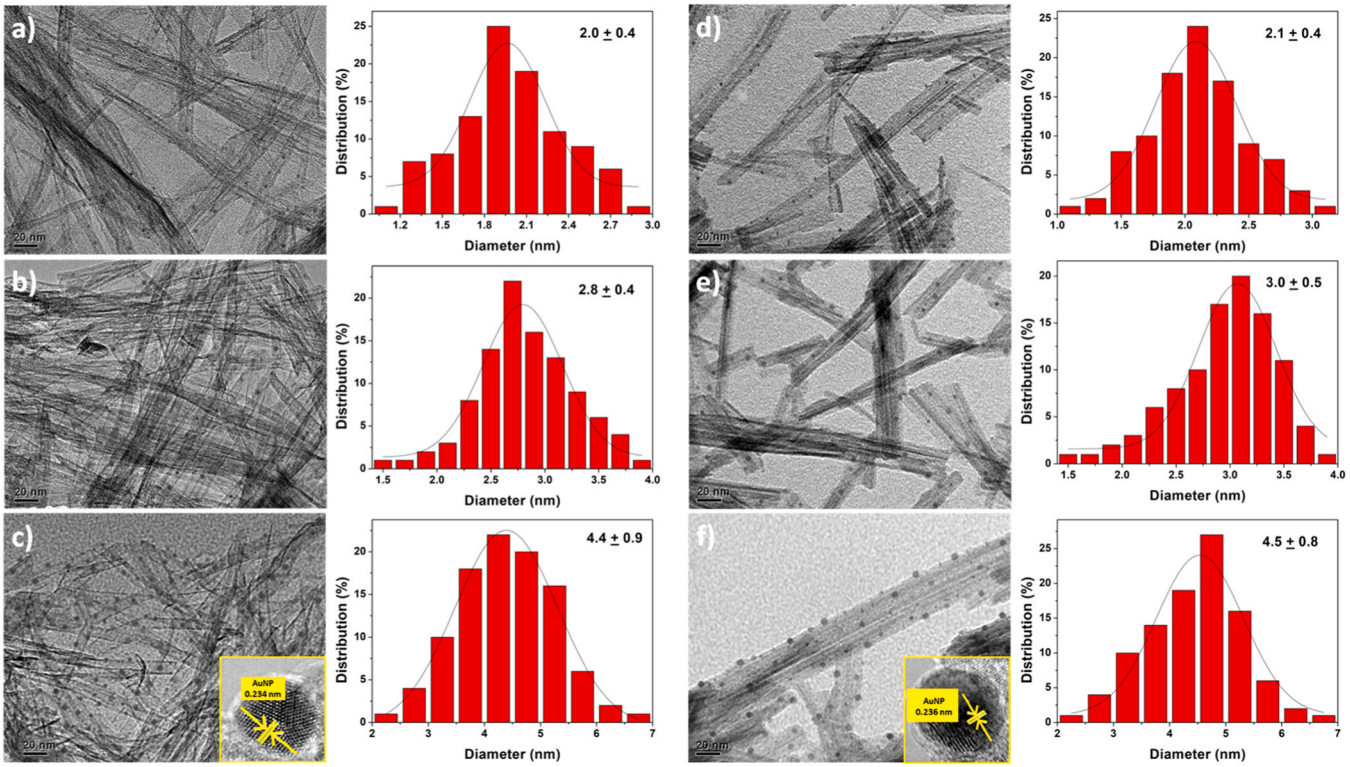


Fig. 3. TEM micrographs of $Au_{1.0}$NPs/HTNTs, b) $Au_{3.0}$NPs/HTNTs, c) $Au_{5.0}$NPs/HTNTs, d) $Au_{1.0}$NPs/HTNWs, e) $Au_{3.0}$NPs/HTNWs and f) $Au_{5.0}$NPs/HTNWs. (Inset shows HRTEM of AuNPs).

nanotubes and nanowires before and after Au impregnation were type IV, which is characteristic of mesoporous materials [44]. Surface modification of the supports with AuNPs led to a decrease in the surface area, volume, and pore diameter. However, the largest decreases in volume and diameter were observed when the Au content reached 3 % and 5 % by mass, respectively. As can be correlated with the particle size determined by TEM, at these metal loadings, the size of the nanoparticles increased between 4 and 5 nm, causing clogging of the internal channels of the tube as the NP grew on the inner surface. The amount of Au supported on the HTNTs and HTNWs was determined by ICP-MS analysis and was found to be very close to the nominal amount. The Au loading on the nanotubes was slightly higher, which could be related to the formation of NPs inside the tubes, trapped in the channels as they grew in size.

The chemical composition on the surface of the samples was investigated from XPS analysis. Fig. S2 (see Supplementary Information) shows the survey spectra of both pristine HTNTs and HTNWs and those loaded with 5 % by weight of Au. In the pristine HTNW samples, signals for Ti, O, C, and Na were observed, showing that residual Na was present on the surface of the nanowires after the alkaline synthesis step. Signals for C were attributed to adventitious C. Following the functionalization with APTMS and Au deposition, Na signals were not observed in the XPS spectrum, indicating that Na was removed from the surface. Other signals associated with Si and N were also observed in the spectrum related to the immobilized APTMS moieties. Finally, an Au signal was observed in the survey spectrum, implying that Au could be fixed on the surface of the catalyst. Similarly, the surface chemical composition of HTNTs and $Au_{5.0}$NPs/HTNTs samples showed a high similarity in the chemical composition to that found on nanowire samples. However, unlike the $Au_{5.0}$NPs/HTNWs sample, the $Au_{5.0}$NPs/HTNTs sample showed Na on the surface, indicating that Na could not be completed removed from the surface after ATPMS immobilization and Au fixation. The high-

Table 1
Summary of textural properties and Au amount and particle size in AuNPs/$H_2Ti_3O_7$ photocatalysts.

Sample	S_{BET} [m^2/g]	Pore volume [cm^3/g]	Pore diameter [nm]	TEM particle size [nm] [a]	Amount of Au [%] [b]	Band-Gap [eV] [c]
HTNTs	382	0.73	6.44	-	-	2.95
$Au_{1.0}$NPs/HTNTs	361	0.70	6.32	2.0	0.98	2.92
$Au_{3.0}$NPs/HTNTs	326	0.64	5.38	2.8	2.96	2.88
$Au_{5.0}$NPs/HTNTs	299	0.56	4.75	4.4	4.95	2.85
HTNWs	318	0.67	8.43	-	-	2.97
$Au_{1.0}$NPs/HTNWs	306	0.65	8.29	2.1	0.96	2.93
$Au_{3.0}$NPs/HTNWs	270	0.61	7.22	3.0	2.94	2.89
$Au_{5.0}$NPs/HTNWs	253	0.53	6.45	4.5	4.90	2.84

[a] Determined by direct NPs measure with ImajeJ software,
[b] Determined by ICP-MS,
[c] Calculated by Kubelka-Munk plot.

resolution spectra of the Ti 2p signal for the four samples are shown in Fig. 4a. As can be seen in this image, the binding energy of Ti $2p_{3/2}$ for supports HTNTs and HTNWs was in the range of 458.4–458.9 eV, indicating that Ti was present as Ti^{+4} in all samples analyzed. However, for the catalysts $Au_{5.0}$NPs/HTNWs and $Au_{5.0}$NPs/HTNTs a discrete contribution of Ti^{3+} centered at 457.7 eV and 457.5 eV was detected, respectively. This confirms that the incorporation of AuNPs on the supports provides the formation of partially reduced Ti^{3+} states by the intimal contact of the metal and the corresponding Ti-based oxides. Fig. 4b shows the high-resolution spectra of the Au 4 f signal of the Au-supported nanowire and nanotube samples. As shown in this image, Au 4 $f_{7/2}$ in both samples was about 83.4 eV, indicating that Au was present on the samples as Au^0 species. No signals associated with Au^{+1} were detected in the high-resolution spectra, confirming that Au^{+1} was completely reduced to Au^0.

The optical absorption characteristics of all samples were determined by UV–vis DRS. As shown in Fig. 5a,b, the pristine HTNTs and HTNWs exhibited a limited light absorption capability only in the ultraviolet region with an absorption edge of 398 and 393 nm for HTNTs and HTNWs, which corresponded to the band-to-band transition of the material [45]. In contrast, for the three Au-loaded supports, a red shift was observed that increased with the amount of Au present in the samples up to 430 nm. This phenomenon of decreasing bandgap of Ti-based supports when composited with AuNPs was previously reported in the literature and attributed to the change in the valence and conduction band energies [46]. After dispersion of AuNPs, the light response range of both AuNPs/HTNTs and AuNPs/HTNWs was extended to visible light as well as enhanced UV light absorption, which was favorable for the photocatalytic effect. The new band around 530–550 nm can be attributed to the localized surface resonance plasmon (LSRP) collective oscillations of "hot electrons" generated on the surface of metallic AuNPs. Photocatalysts with a higher amount of dispersed Au exhibit a greater red shift, due to a larger particle size [26]. Furthermore, these results are in agreement with the TEM observations, where the supports with 5 % Au were seen to have the largest particle sizes. The bandgap energies of the obtained Au nanocomposites were estimated using the relationship between the Kubelka–Munk function and the photon energy, as shown in Fig. 5c,d. The bandgap energies for the bare HTNTs and HTNWs were 2.95 and 2.97 eV, respectively. Additionally, the bandgap energies were found to be 2.92, 2.88, and 2.85 eV for the prepared AuNPs/HTNTs nanocomposites with 1.0 %, 3.0 %, and 5.0 % of Au, and 2.93, 2.89, and 2.84 eV for the AuNPs/HTNWs with 1.0 %, 3.0 %, and 5.0 % of Au, respectively. The charge delocalization was caused by the contact between the phases, generating an electronic recombination that favors the passage of electrons from the valence band to the conduction band of the photocatalyst. This decrease in energy could favor forbidden transitions, and it could be assumed that the catalyst could be more visible radiation.

Fig. 6a,b show the photoluminescence (PL) spectra for the different AuNPs/HTNTs and AuNPs/HTNWs photocatalysts and reveals that the electron–hole pair recombination in both HTNTs and HTNWs supports was progressively inhibited with increasing Au loading. All samples exhibited two emission peaks in the UV–vis region. The UV emission centered at 390 nm is related to the electron transition from the valence band to the conduction band, and the emission centered at about 600 nm may result from the recombination of photogenerated holes with the electrons in singly occupied oxygen vacancies [47]. The decrease in the PL intensity reflects a reduction in electron-hole recombination, which is induced by the transfer of electrons

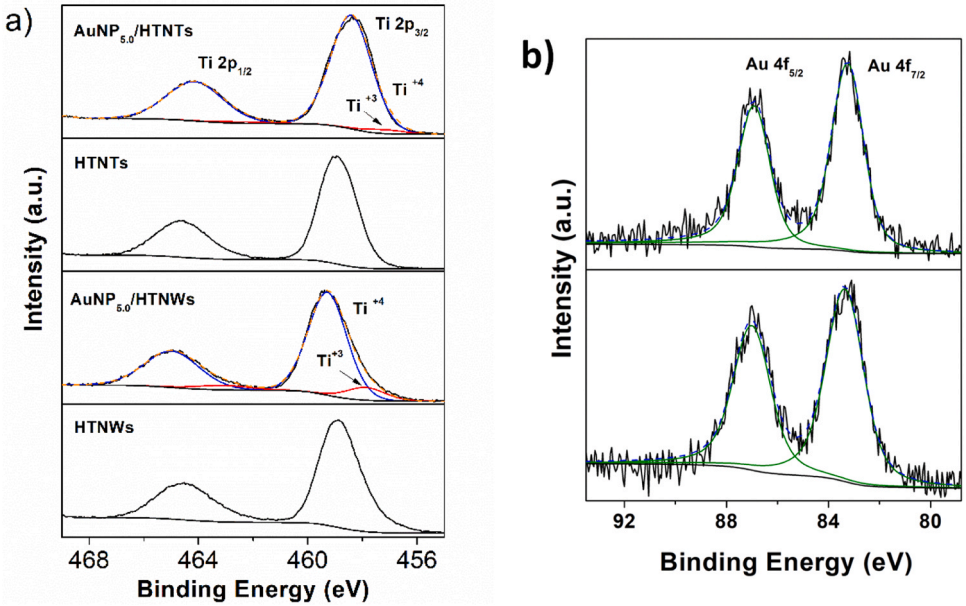


Fig. 4. high-resolution X-ray photoelectron spectra (XPS) of a) Ti 2p and b) Au 4 f.

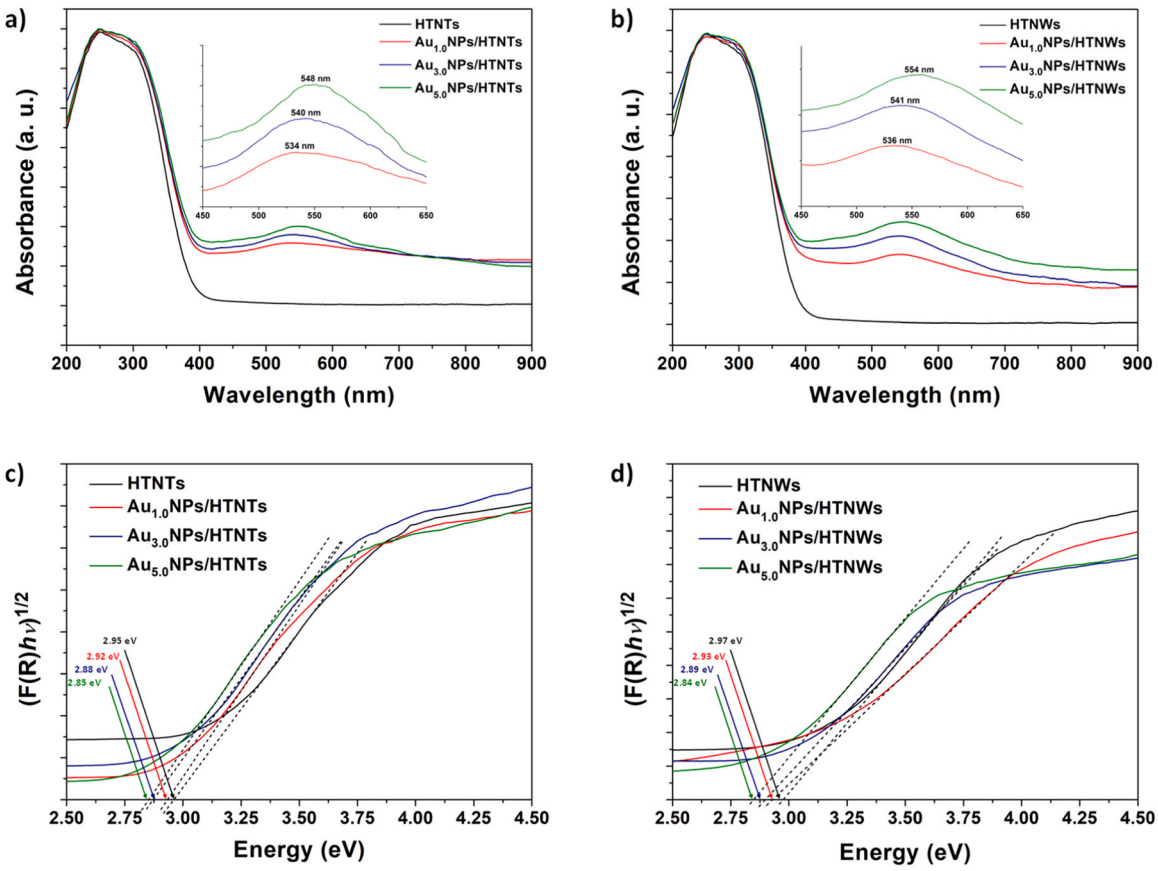


Fig. 5. UV-Vis DRS of a) AuNPs/HTNTs and b) AuNPs/HTNWs; Kubelka-Munk plot of c) AuNPs/HTNTs and d) AuNPs/HTNWs.

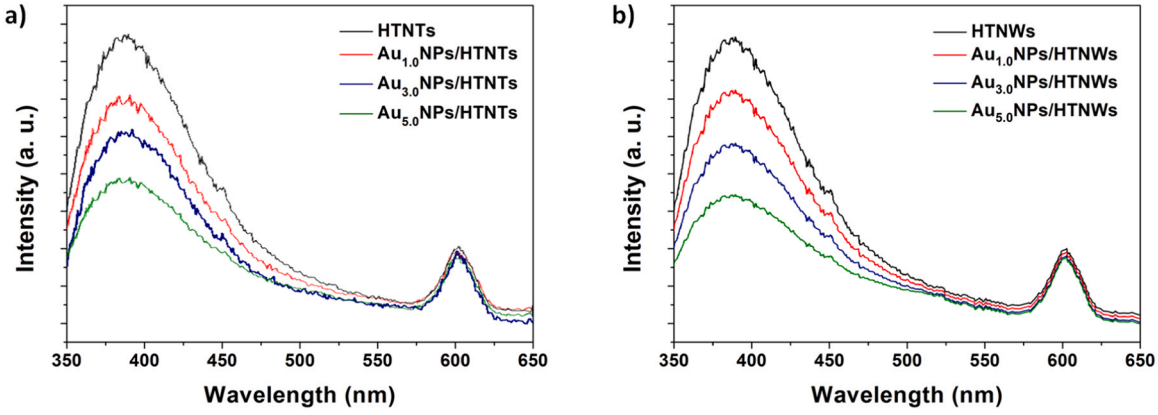


Fig. 6. PL spectra of a) AuNPs/HTNTs and b) AuNPs/HTNWs photocatalysts.

photogenerated in the Au-doped HTNTs and HTNWs s to the AuNPs. This charge separation is crucial for achieving high photocatalytic performance [48]. The PL intensity was shown to have a direct linear relationship with the absorbance maximum for each photocatalyst. The results suggest a very close relationship between the optical properties, related to the LSPR absorbance of gold, and the charge separation properties of the AuNPs/HTNTWs and AuNPs/HTNTs photocatalysts [49].

To further elucidate the electronic band energies of bare HTNTs and HTNWs and Au-supported catalysts, Mott–Schottky (MS) measurements were performed to elucidate the flat band (E_{FB}), valence band (VB), and conductance band (CB) potentials. As shown in Fig. 7a,b, the positive slope in the MS plot for the HTNTs and HTNWs and AuNPs/$H_2Ti_3O_7$ solids indicates that the n-type behavior of $H_2Ti_3O_7$ is retained in Au-loaded catalysts [50,51]. The flat band potential was determined by extrapolating the X-intersections in the MS plots and were recorded as −1.00 and −0.99 V for HTNTs and HTNWs, respectively, versus the Ag/AgCl electrode, respectively. Using the Nernst equation $E_{NHE} = E_{Ag/AgCl} + 0.1976$ V (25 °C) [52,53], the E_{FB} can be converted to −0.80 and 0.79 V vs the normal hydrogen electrode (NHE). The valence band (VB) positions were calculated considering that E_{FB} is the Fermi level for n-type semiconductors; therefore, the VB value was the same (1.93 V vs NHE) for both HTNTs and HTNWs supports. The results of the valence band XPS (VBM) spectra measurements of the investigated materials are shown in Fig. 7c,d. The energy gap between the BV and the Fermi level was recorded as 2.74 and 2.72 for HTNTs and HTNWs,

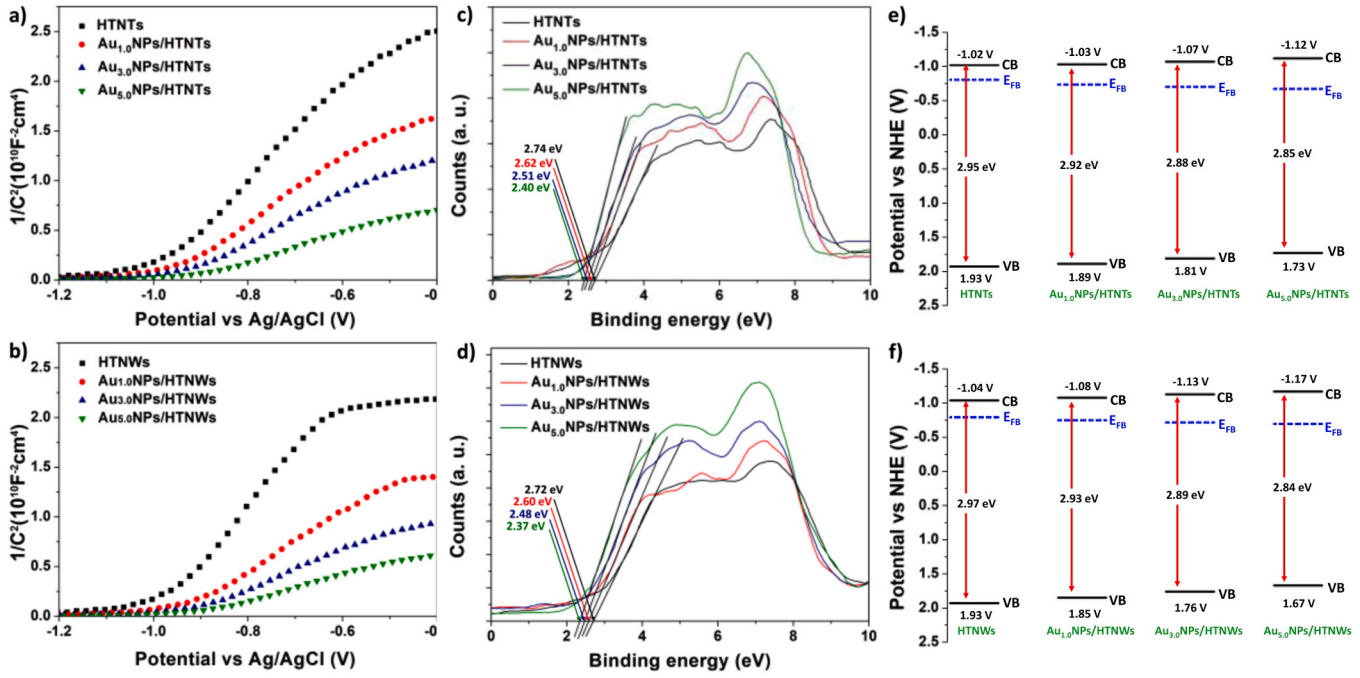


Fig. 7. Mott-Schottky plots of a) AuNPs/HTNTs and b) AuNPs/HTNWs; XPS valence band spectra of c) AuNPs/HTNTs and d) AuNPs/HTNWs; band structure alignments of e) AuNPs/HTNTs and f) AuNPs/HTNWs.

respectively [54,55]. Thus, using the band gap energy values obtained by Kubelka–Munk plots, the band energy diagram (shown in Fig. 7e,f) can be constructed. The same calculations were used to determine de VFB and VB for the Au-loaded catalysts to gain insights into the effect of Au loading on the photocurrent density. The values of V_{FB} were compared with respect to the Fermi level of ~5 nm Au particles deposited on $H_2Ti_3O_7$ support. The Femi level of 5 nm of AuNPs was about –0.45 V vs. RHE [56]. Therefore, when AuNPs were irradiated

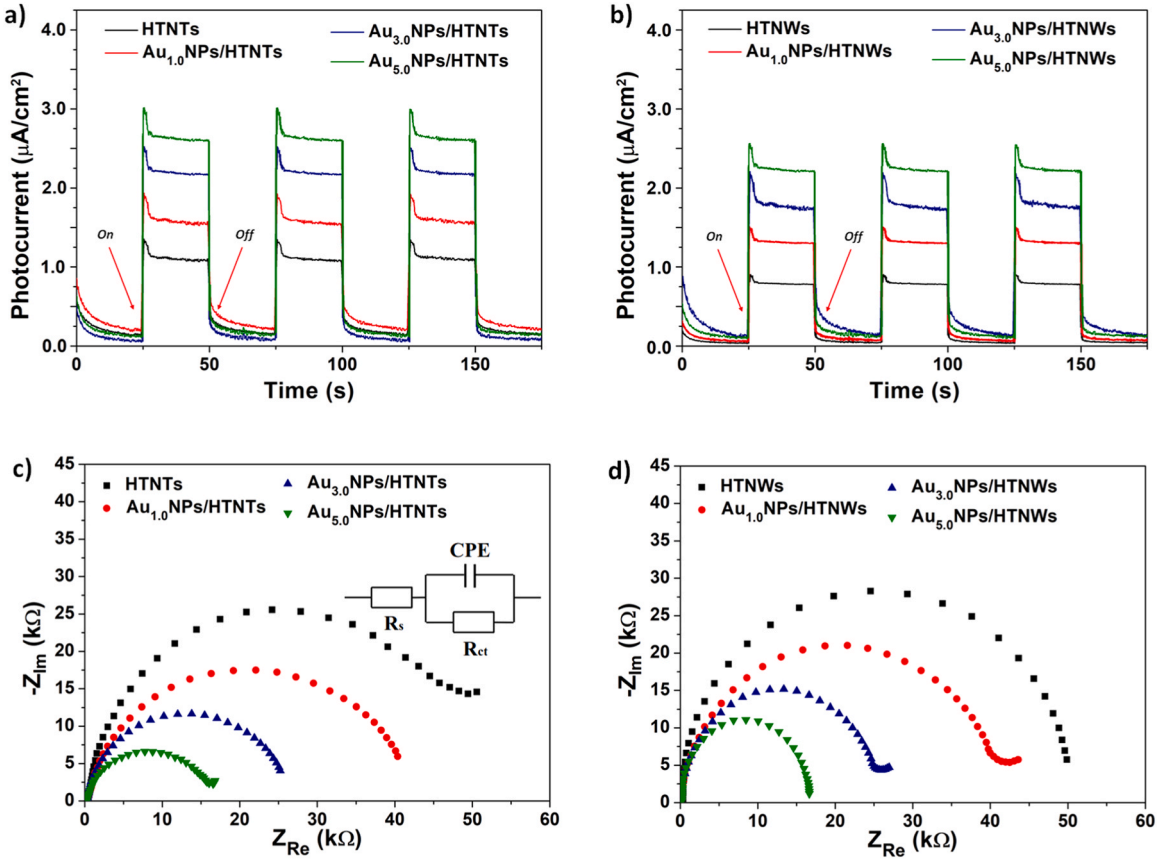


Fig. 8. Photocurrent response of a) AuNPs/HTNTs and b) AuNPs/HTNWs; Nyquist impedance spectrograms of c) AuNPs/HTNTs and d) AuNPs/HTNWs.

with visible light, "hot electrons" were generated by the LSPR effect, which easily migrated to the conduction band of the $H_2Ti_3O_7$ support. Additionally, the VBM results showed that the Au-loaded solids shifted proportionally to the amount of Au deposited toward lower binding energies compared to bare $H_2Ti_3O_7$ supports. The shift occurred due to charge transfer and the formation of a Schottky barrier height (SBH) at the interface between the support and the AuNPs [57]. Moreover, the variation in the intensity of the photoelectron emission reflects a different surface electronic structure of the investigated samples. The spectral structure in the energy range of 0–10 eV was the valence band structure and reflected the valence band density of states of the $H_2Ti_3O_7$ phase. The valence band edges of the samples were dominated by O 2p emission [58]

To measure the difference in charge transfer of the photocatalysts in the presence of visible light, transient photoresponse spectroscopy was performed in the presence and absence of visible radiation. As shown in Fig. 8a,b, all the solids were sensitive to visible light, with the photocurrent increasing and decreasing as the radiation source was turned on and off and were also shown to have relatively stable performance. The photocurrent density response was found to increase with the amount of Au present in the HTNTs and HTNWs, confirming the role of Au to prevent recombination of photogenerated charges [53]. That is, photocatalysts with 5 % by mass of Au have the best separation efficiency of photogenerated electrons and photogenerated holes in the support [45, 51,59,60]. To complement the electrochemical characterization, EIS analysis was performed. Fig. 8c,d show the Nyquist diagrams of the different electrodes modified with the photocatalysts after irradiation with visible light. The results show that the arc radius decreases with the amount of Au incorporated in the support, indicating that the addition of Au decreases the resistance to charge transfer, which is reflected in a lower recombination rate [45,51,60]. These results are consistent with the trend observed in other electrochemical measurements, such as photocurrent and PL results. In general, the results of the electrochemical characterization demonstrate that the preparation method of functionalization with APTMS and subsequent deposition of Au and reduction with $NaBH_4$ allows to obtain photocatalytic systems sensitive to visible light.

3.2. Photooxidation of Lignin-based alcohols

$H_2Ti_3O_7$ supports modified and unmodified with Au were evaluated for the selective photooxidation of model solutions of lignin-derived alcohols prepared in CH_3CN. The photoreactions were carried out under visible light (λ>400 nm), bubbling O_2, at 20 °C and 300 rpm stirring. The time evolutions of the photoconversion of vanillyl and veratryl alcohols using AuNPs/HTNTs and AuNPs/HTNWs are shown in Fig. 9. First, the catalyst mixture was stirred until the adsorption equilibrium was reached. Tests were performed without light, with light and without catalyst (photolysis), and only with the unmodified $H_2Ti_3O_7$ supports. In all cases, the conversion did not exceed 10 %, indicating that the presence of both light and Au as antenna for the visible light absorption is necessary. Consistently, for both solids, the conversion increased with the amount of Au present in each support. Fig. 9a shows that the $Au_{5.0}$NPs/HTNTs system approached 100 % conversion of vanillyl alcohol after 6 h of visible-light irradiation. The results showed a slight decrease in the conversion when Au catalysts supported on HTNWs were used. It was also observed that the conversion decreased when veratryl alcohol was evaluated, which was related to the

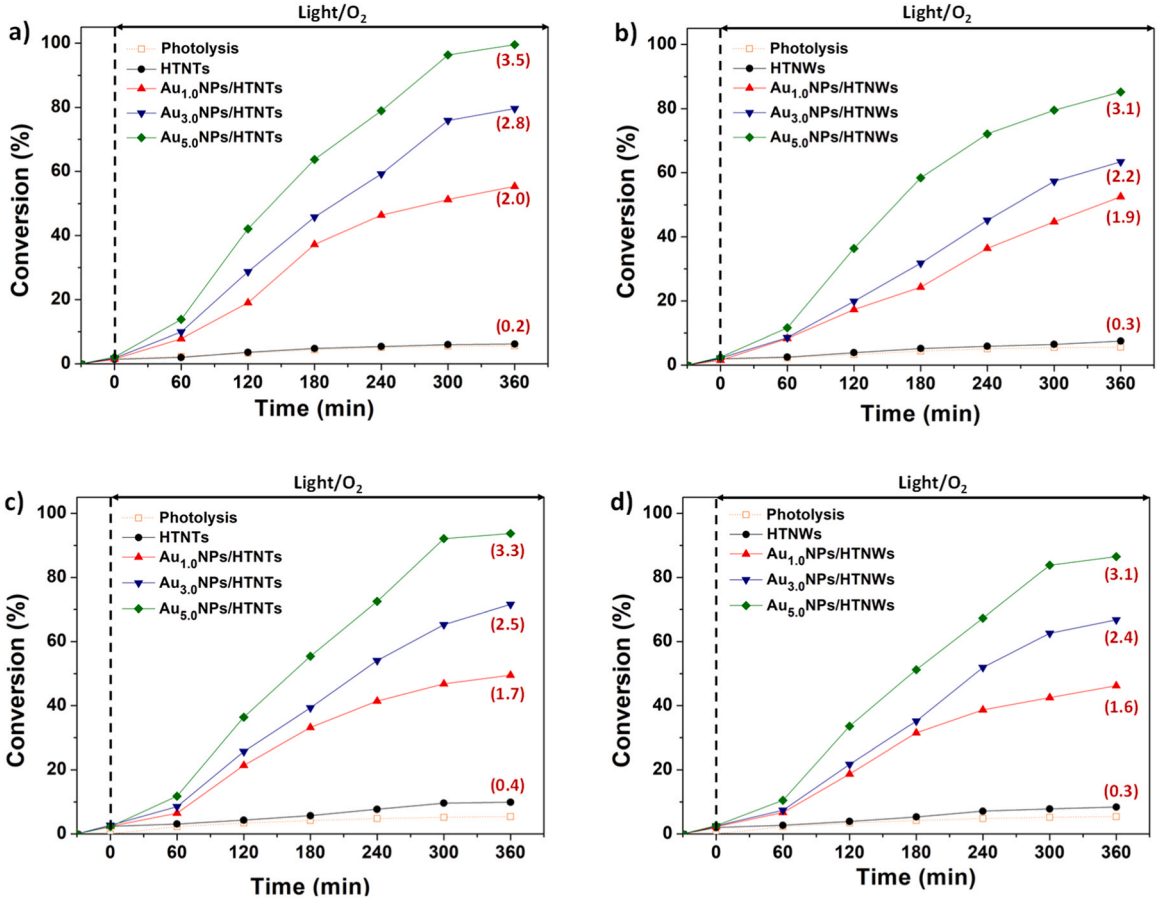


Fig. 9. Vanillyl alcohol photoconversion versus time using a) AuNPs/HTNTs and b) AuNPs/HTNWs and veratryl alcohol photoconversion versus time using c) AuNPs/HTNTs and d) AuNPs/HTNWs.

substituents on the aromatic ring and the intermediates present in the reaction [61]. It is important to highlight that in all cases, a selectivity of 99 % was obtained toward the formation of the corresponding aldehyde, with negligible prodcution of acid derivative as a byproduct. The high selectivity toward aldehyde formation in the selective oxidation of benzylic-derived alcohols using AuNPs supported on HTNTs as catalyst, oxygen as primary oxidant, and visible light as activation source is due to a combination of key factors: (a) Au in nanoparticle form exhibits significant catalytic activity, especially in visible light driven oxidation reactions, and the size and shape of AuNPs can be controlled during their synthesis tunning the light absorption, (b) HTNTs provide a high surface area, allowing good dispersion of AuNPs and increased exposure of the active sites while the presence Ti-OH surface groups can modulate the selectivity to the target product; Additionally, the oxidation reaction with oxygen can be directed toward the formation of specific products depending on the reaction conditions, and (c) the energy provided by the visible light and the catalyst–substrate–oxidant interaction is adjusted to promote the desired oxidation at a reasonable rate under mild conditions and to avoid over-oxidation to other products. Furthermore, the photonic efficiencies of the different catalytic systems (red values given in parentheses to the right of each reaction figure) were determined using the number of moles of aldehyde obtained at the end of the reaction (mol s^{-1}) and the photonic flux (Einstein s^{-1}) [62, 63]. The type of support morphology does not seem to have an important effect on photocatalytic activity, considering that the two morphologies correspond to 1D structures with high surface area/volume ratios. It is evident that the pristine supports are less active in the reactions promoted by visible light than the catalysts. This trend is consistent with the electrochemical characterization and suggests that the method of preparation of the photocatalysts allows obtaining nanocomposites that are active against the selective oxidation of alcohols using visible light and that the incorporation of Au on the surface of the support and subsequent reduction with $NaBH_4$ generates defects on the surface. Furthermore, the sequential Au incorporation method can generate relatively small particle sizes for significant Au loadings (5 % w/w), all of which are reflected in an improvement in photonic efficiency.

The $Au_{5.0}$NPs/HTNTs photocatalyst with superior catalytic activity was evaluated in the photo-oxidation of various benzylic-derived substituted alcohols to determine its applicability. As shown in Table 2, the conversions of 4-methyl (entry 2), 4-hydroxy (entry 3), 4-methoxybenzyl alcohol (entry 4), 3,4-dimethoxybenzyl alcohol (entry 5), 4-hydroxy-3-methoxybenzyl alcohol (entry 6), and 3,4,5-trimethoxybenzyl alcohol were 98.3 %, 99.2 %, 98.9 %, 93.7 %, 99.5 %, and 81.4 %, respectively, which is much higher than the conversion of 64.1 % found for benzyl alcohol (entry 1). In contrast, lower conversions to benzyl alcohol were found for 4-nitro (entry 8), 4-chloro (entry 9), and 4-cyanobenzyl (entry 10) alcohols at 39.8 %, 54.0 %, and 50.5 %, respectively.

In order to predict a possible reaction pathway for the photo-oxidation of alcohols with O_2 catalyzed by the $Au_{5.0}$NPs/HTNTs system, various *p*-substituted benzyl alcohols were evaluated using the Hammett methodology [64,65]. Fig. 10 shows the variation of the logarithm of the rate constants with respect to the Hammett (σ) and Brown–Okamoto (σ^+) parameters for each substituent. A linear correlation was observed between the $\log(k_x/k_H)$ values and the σ^+ parameters with a negative slope (ρ=1.01, r^2=0.9975). This clearly shows that positive charge accumulation occurred in the substrate activation step. This suggests that the rate-determining step transition state developed a partial positive charge on the benzyl carbon, which was stabilized by resonance through electron-donating substituents (−CH_3, −OCH_3,

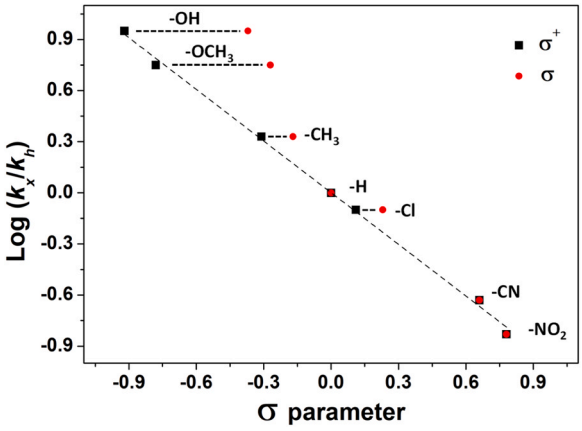
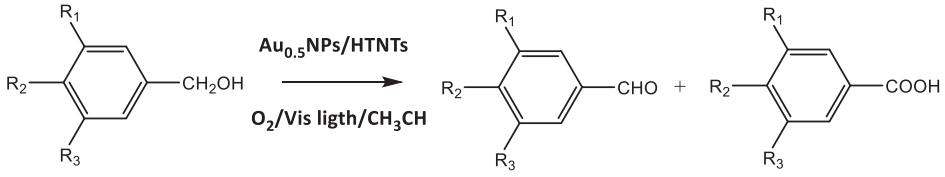


Fig. 10. Hammett-type plots for the photooxidation of benzyl alcohol and *p*-substituted benzyl alcohols. Reaction conditions: substituted benzyl alcohols (5 mmol), 30 mg $Au_{5.0}$NPs/HTNTs, 300 rpm and O_2 under vis light for 6 h.

Table 2
Selective photo-oxidation of various lignin-derived alcohols using $Au_{5.0}$NPs/HTNTs catalyst with O_2 under Vis light.



(1) (2) (3)

Entry	R_1	R_2	R_3	Conversion (%)	Selectivity (%)	
					(2)	(3)
1	H	H	H	64.1	99	1
2	H	CH_3	H	98.3	98	2
3	H	OH	H	99.2	97	3
4	H	OCH_3	H	98.9	98	2
5	OH	OH	H	93.7	99	1
6	OCH_3	OH	H	99.5	99	1
7	OCH_3	OCH_3	OCH_3	81.4	95	5
8	H	NO_2	H	39.8	94	6
9	H	Cl	H	54.0	96	4
10	H	CN	H	50.5	95	5

Reaction conditions: 0.1 M alcohol solution, using 30 mg of $Au_{5.0}$NPs/HTNTs catalyst, 300 rpm, Vis light (λ> 400 nm) and O_2 after 6 h.

−OH) on the phenyl ring [66]. This fact explains why vanillyl and veratryl alcohols show higher reactivity compared to benzyl alcohol. These results suggest that the loss of hydrogen from benzyl carbon is the rate-determining step in the oxidation of benzyl alcohol over this type of supported Au catalyst. Previously, it has been reported for similar systems that density functional theory (DFT) calculations also suggest that deprotonation of alcohol is required, consistent with the literature on homogeneous catalysts [64,67].

To study the effect of the type of radiation, the oxidation of vanillyl alcohol with O_2 was carried out in the presence of UV light using the $Au_{5.0}$NPs/HTNTs catalyst. As shown in supplementary material Table S1 (entry 1), 100 % conversion was achieved after 4 h of reaction. However, the selectivity toward vanillin formation decreased to 84 %. Irradiation of such systems with UV light generates electronic transitions from the valence band to the conduction band of the support; in this case, the electrons are injected from the support to the Au [68] and the oxidation reactions are promoted by the photoholes generated in the valence band of the support, which possess a higher oxidation potential enabling the production of over-oxidize products as vanillic acid. Fig. S4 shows the photo-conversion of vanillyl alcohol under the same conditions as the previous reactions, under green visible light (300 W Xenon arc lamp, Newport, Oriel LH300). As expected, the energy of the green radiation (longpass optical filter transmitting UV-light with $\lambda > 480$ nm was used) is enough to generate the surface resonance plasmon effect on AuNPs, in agreement with the previous characterization. In the first two hours of reaction, the conversion was higher when green radiation was used. This effect is related to the time it takes for the radiation source to reach its maximum emission. Another method of sonochemical activation at low frequency (20 kHz) was carried out in the presence of UV (Table S1, entry 2) and visible light (Table S1, entry 3), and the combination of these two activation sources is known as sonophotocatalysis. The joint use of radiation with ultrasound and light decreased the reaction times to 3 h to obtain 100 % conversion, but the selectivity to vanillin decreased. It was observed that the longer the reaction time, the higher the formation of vanillic acid. Previous reports have demonstrated this improvement in catalytic performance when using low-frequency ultrasound [69], which generated physical effects in the reaction medium that increased the mass transfer phenomena between O_2, the substrate, and the catalyst.

The effect of different scavengers on the photo-oxidation reaction of vanillyl alcohol was studied: 1,4-benzoquinone (BQ) for $O_2^{\bullet-}$, dimethyl sulfoxide (DMSO) for ·OH, formic acid for photoholes (h^+), and silver nitrate ($AgNO_3$) for photoelectrons (e^-) [55,70]. Fig. 11a shows the conversion and selectivity of the different photoreactions. In the presence of BQ, the conversion decreased by more than 50 %, due to the competitive reaction between BQ and vanillyl alcohol to react with the superoxide radical anion ($O_2^{\bullet-}$). On the other hand, in the presence of DMSO and formic acid, no significant changes in photocatalytic activity were observed. Moreover, while the conversion of formic acid was moderately high (<70 %), the conversion of DMSO was minimal (<10 %), indicating the presence of H^+ in the photocatalyst and the low concentration of −OH in the reaction medium, considering that the reaction was carried out in CH_3CN. Finally, when a AgNO3 solution was added, the conversion decreased drastically, indicating that the Ag^+ cation competed with O_2 to capture the hot electrons generated in the AuNPs when irradiated with visible light. In the same direction, electron paramagnetic spectroscopy (EPR), a useful tool for studying electron transfer in semiconductors [71], was performed to determine the presence of species with unpaired electrons, such as radicals, crystalline defects and free and trapped charge carriers. Fig. 11b shows the EPR spectra of the HTNTs support, both pristine and 5 %-Au-modified, both in the dark and in visible light at 90 K under Ar. In both light and dark, the HTNTs did not show any characteristic signal indicating photoexcitation of the support in the absence of AuNPs. Contrarily, when AuNPs were incorporated into the support, two new signals were observed, evidencing the electron transfer and, therefore, the sensitivity of the

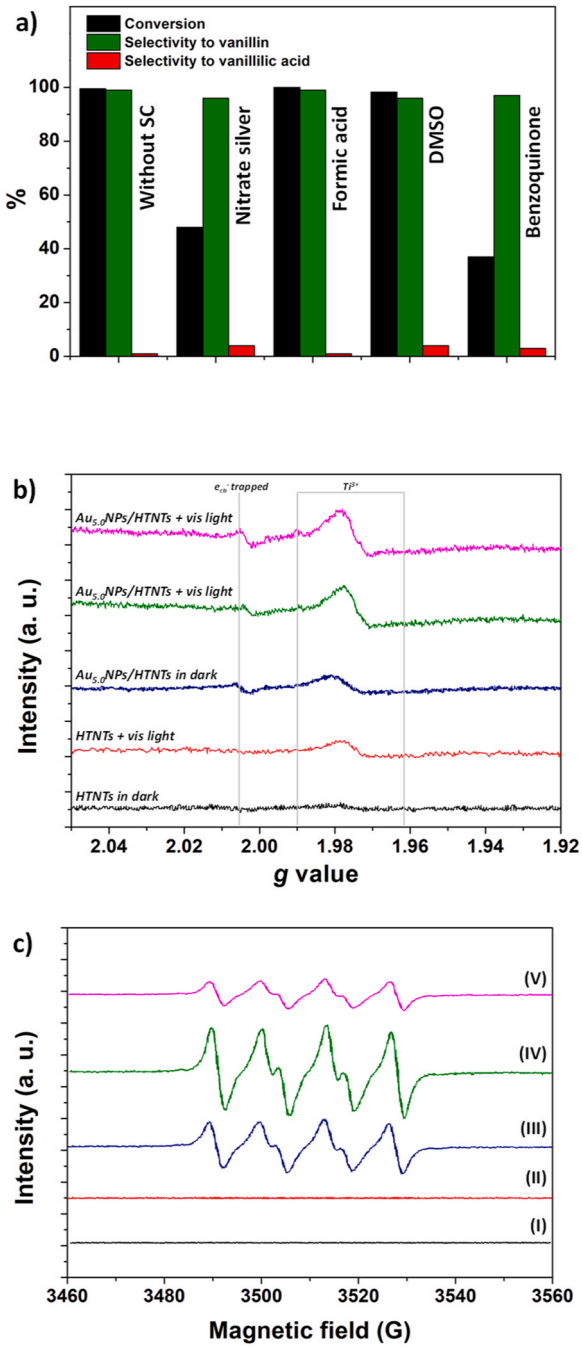


Fig. 11. a) Conversion and selectivity in the photo-oxidation of vanillyl alcohol with 0.1 M alcohol solution in the presence of different scavengers 50 mM, using 30 mg of $Au_{5.0}$NPs/HTNTs catalyst, 300 rpm, vis light and O_2 after 6 h; b) EPR spectra of pristine and Au-modified HTNTs catalysts at 90 K in Ar and c) DMPO-trapping EPR spectra of DMPO–$O_2^{\bullet-}$ under visible light irradiation with pristine and Au-modified HTNTs.

catalyst to visible light.

The anisotropic signal at g= 1.990 could be attributed to the reduction of Ti^{4+} to Ti^{3+} mediated by the LSPR photogenerated electrons from the AuNPs being trapped by the support [72]. The signal at g = 2.005 was also attributed to the electrons trapped in the oxygen vacancies. According to the above characterization it was observed that the while $H_2Ti_3O_7$ support was not sensitive to visible light, AuNPs could absorb visible light, facilitating the injection of photoelectrons into the conduction band of the support. In this sense, the oxygen vacancies acted as a trap for the photogenerated electrons [73]. Additionally, EPR

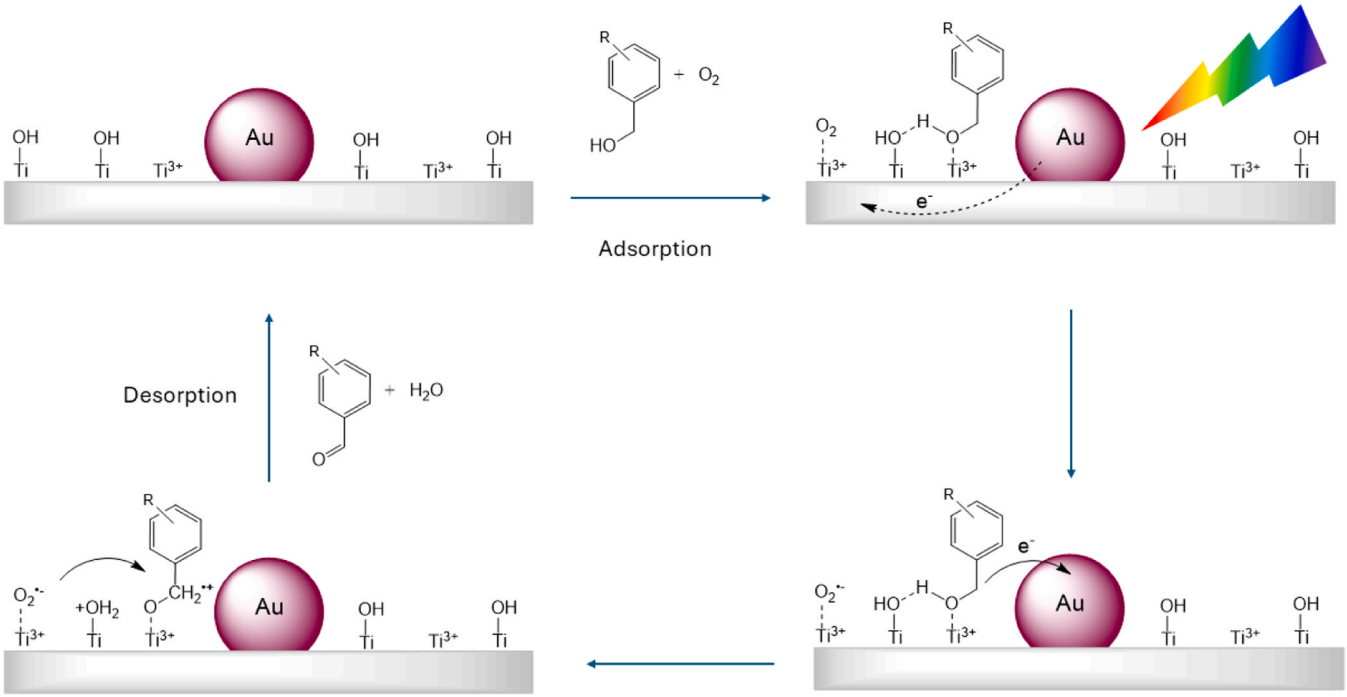
measurements were performed using on the pristine support of HTNTs and $Au_{5.0}$NPs/HTNTs in vanillyl alcohol solution and O_2 bubbling in the presence of DMPO as a trapping agent for $O_2^{\bullet-}$ radicals. Fig. 11c shows that both the Au-modified catalytic system in the dark (I) and the pristine support in the presence of visible light (II) displayed no signal. On the other hand, when the Au-modified system was irradiated with visible light (III, IV), four characteristic signals of the DMPO- $O_2^{\bullet-}$ adduct appeared [74], and their intensity increased with the irradiation time. Finally, when $AgNO_3$ was added to the reaction medium, the intensity of the signals decreases drastically. These results agree with those results observed in the reactions with scavengers, corroborating that electrons are generated by the action of visible light on the AuNPs and are transferred to the conduction band of the support. Furthermore, the addition of Ag^+ ions trapped the generated photoelectrons, confirming that they play a fundamental role in the photocatalytic reaction as reflected in the conversion of the substrates.

Considering the results obtained and the possible ways of adsorption of benzyl alcohol derivatives on Au/TiO_2-type catalysts reported previously, a possible reaction pathway is proposed. It is well known that −OH groups on the surface of metal oxides play an important role in the adsorption of alcohols [75,76]. Previous work involving DFT calculations has determined the interaction modes of benzyl alcohol with surface hydroxyl groups. However, in our case, the intimal contact with the AuNPs is necessary for the effective electron transfer from the benzyl carbon with the consequent loss of hydrogen because the AuNPs act as antenna under visible light irradiation. Scheme 1 proposes the possible mechanism for the selective photooxidation of the benzylic alcohols scaffolds: Adsorbed O_2 species are the traps for electrons to produce $O_2^{\bullet-}$. Then, the adsorbed alcohol species in CH_3CN transfer electron to the AuNPs forming the radical cation. The oxidation process takes place via interaction with the $O_2^{\bullet-}$ producing the target product.

The highest selectivity displayed is a consequence of the adsorption of the benzylic alcohol on the Ti-based support. To confirm this hypothesis, Fig. S5 shows the evolution of the FT-IR spectrum of the $Au_{5.0}$NPs/HTNTs catalyst over time during the first minutes of the vanillyl alcohol oxidation. The characteristic signals of vanillyl alcohol and vanillin were observed. The increase in the signal intensity is related to the evolution of the reaction in time, evidencing the detection of the adsorbed species. alcohol with the formation of a stable alkoxide species in the catalyst surface. The formation of this transition state with a partial positive charge on the benzylic carbon was previously predicted by Hammett analysis. The α-C-H interacts with $O_2^{\bullet-}$ and dissociates to form the corresponding benzaldehyde [77,78].

To confirm the recyclability of the $Au_{5.0}$NPs/HTNTs photocatalyst, it was reused in 10 catalytic cycles of vanillyl alcohol using the same experimental conditions. For this purpose, the solid was filtered, washed, and dried at the end of each reaction. Fig. 12a shows the catalytic activity for each of the reuse cycles of the photocatalyst. The recycling tests confirmed the stability of the Au dispersion method on the HTNTs support to be used up to seven cycles without altering its photocatalytic activity. At the end of the tenth cycle, a 36 % decrease in vanillyl alcohol in the conversion was observed, while the selectivity toward vanillin was maintained. TEM images of the photocatalyst after the tenth reaction cycle allowed to correlate the loss of activity with an increase in the size of the AuNPs to an average of 6.3 nm (Fig. 12b). ICP-MS analysis of the recovered catalyst revealed a decrease in the metal loading from 4.9 % in mass to 3.8 %Au leached. This confirms the occurrence catalyst deactivation during recyclability studies, which was attributed to the sintering of Au-NPs and the leaching to the liquid phase.

The selective oxidation of vanillyl alcohol with TBHP, air, and O_2 as oxidants under different experimental conditions has been extensively studied over Au catalysts, as summarized in Table 3. AuNPs are supported on many materials such as metal–organic framework (MOF), Al_2O_3, ZnO, and TiO_2. The examples in Table 4 show the thermal or photocatalytic activation of O_2. The present $Au_{5.0}$NPs/HTNTs catalyst is found to be the most active and selective in the literature to date, under relative mild reaction conditions. Entries 1–7 require temperatures at or above 80 °C to activate the oxidizing agent. The most important catalytic results were found for Au/ZnO catalysts (entry 3) using *p*-xylene as solvent and 24 h of reaction and Au-$Pd_{1.2}$@γ-Al_2O_3 (entry 6), where the presence of Pd significantly enhanced the catalyst activity. The photocatalytic oxidation of vanillyl alcohol has also been evaluated with the Au-Pd@HT-PO_4^{3-} system. However, the conversion and selectivity obtained has been moderate in 24 h reactions. These results strongly depend on the size, dispersion, and electronic properties of the AuNPs



Scheme 1. Possible process of benzyl-type alcohols photooxidation mediated by AuNPs/HTNTs catalysts.

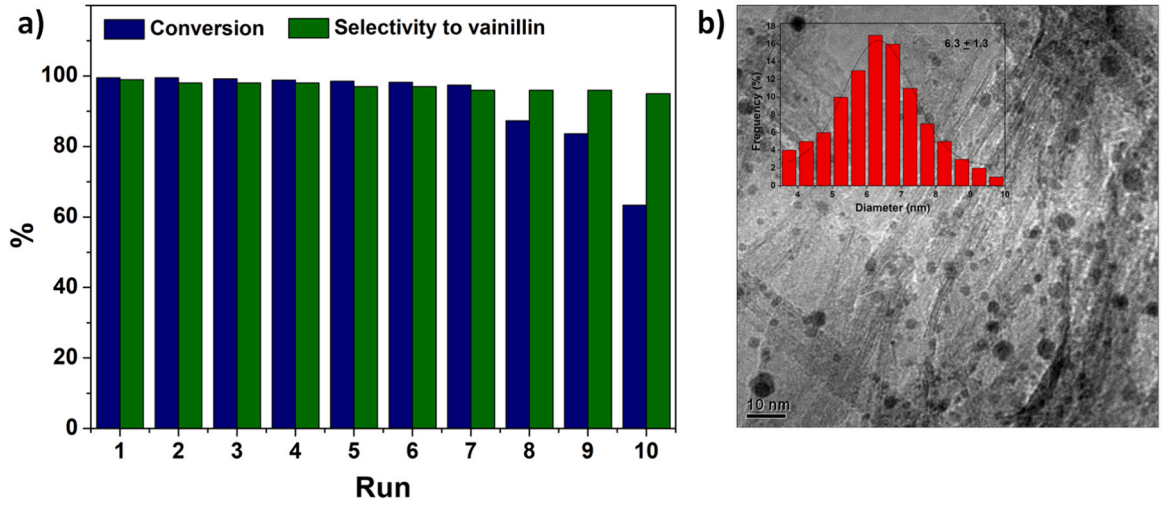


Fig. 12. a) Catalytic stability of AuNPs/HTNTs for the selective photo-oxidation of vanillyl alcohol (b) TEM micrograph of used catalysts after 10 recycles.

Table 3
Comparison of the catalytic performances of the Au-NPs supported for the oxidation of vanillyl alcohol to vanillin.

Entry	Catalyst	Conv. [%]	Sel. [%] [a]	Reaction conditions				Ref.
				T [°C]	Time [h]	Solvent	Oxidant	
1	Au/Al_2O_3	87	87	80	8	Toluene	TBHP	[79]
2	Au@UiO−66(Ce)	43	90	60	8	CH_3CN	TBHP	[80]
3	Au/ZnO	100	100	120	24	*p*-xilene	O_2	[11]
4	Au/CeO_2	73	83	80	7	H_2O	O_2	[13]
5	$Au@Rb_9Cu_6(P_2O_7)_4Cl_2$	42	56	170	10	*t*-BuOH	air[b]	[81]
6	$Au\text{-}Pd_{1.2}@\gamma\text{-}Al_2O_3$	99	99	80	2	H_2O	air	[82]
7	Au/TiO_2	35	99	80	0.5	H_2O	O_2	[12]
8	$Au–Pd@HT\text{-}PO_4^{3-}$	53	50	Ta[c]	24	Dioxane	air	[83]
9	$Au_{5.0}$NPs/HTNTs	99	99	Ta[c]	6	CH_3CN	O_2	*This work*

[a] Selectivity to vanillin,
[b] P_{air} (20 °C) = 20 bar,
[c] Photocatalytic reaction at 25 °C and P atm.

and the metal–support interaction (MSI) and the nature of the support. Comparison of the results suggests that our methodology allows the use of O_2 at low temperature (25 °C) under visible light (λ> 400 nm) with a high activity, selectivity and stability toward vanillin at 6 h under base-free conditions.

4. Conclusions

The functionalization of HTNTs and HTNWs with APTMS and subsequent Au dispersion and reduction with $NaBH_4$ allowed efficient and stable photocatalytic systems for the photooxidation of lignin-derived benzyl-type alcohols toward their respective aldehydes using O_2 as the oxidant and visible light as the driving source of the reaction at room temperature. By successively dispersing Au on the support, it was possible to obtain up to 5 % Au by mass while maintaining high dispersion and an NP size of approximately 4 nm. Increasing the amount of Au in the support increased the number of defects in the solid, which affected the photocatalytic efficiency of the reaction. The favorable photocatalytic activity of the AuNPs/HTNTs and AuNPs/HTNWs systems was due to several factors that contributed to their enhanced photocatalytic performance. These include the 1D morphology of the supports, generation of oxygen vacancies, and Ti^{3+} species that are generated upon the modification of titanates with AuNPs. The catalytic activity of the prepared system was enhanced by the plasmonic activity of the AuNPs because of the electrochemical characterizations performed (photoluminescence, MS measurements, photocurrent response), which demonstrated the generation of an electronic current from the catalyst to the O_2 adsorbed to favor the oxygen superoxide formed with visible radiation. Additionally, the reaction scheme was explained using the observed catalytic data together with the electrochemical characterization, and EPR and XPS results. In summary, this experimental study contributes to the plasmonic photocatalysis of supported AuNPs for selective oxidation reactions.

CRediT authorship contribution statement

Torres Cecilia C: Writing – review & editing, Project administration, Methodology, Funding acquisition. **Campos Cristian H:** Writing – review & editing, Data curation, Conceptualization. **Álvaro A. Amaya:** Investigation, Formal analysis. **Martinez Fernando:** Writing – review & editing, Formal analysis. **Henry Martínez:** Writing – original draft, Visualization, Project administration, Investigation, Funding acquisition, Formal analysis.

Declaration of Competing Interest

The authors declare that they have no known competing financial interests or personal relationships that could have appeared to influence the work reported in this paper.

Acknowledgements

The author (H. M.) thanks to FONDECYT-ANID Postdoctoral Grant 3230341 (Chile), C. C. Torres to FONDECYT-ANID Grant 1231395

(Chile) for the financial support, and the author (F.M.O.) thanks to Laboratorio Central en Ciencia de Superficies (SurfLab-UIS) for providing the facilities to carry out the XPS measurements at the Universidad Industrial de Santander. We would like to thank the Institute of Applied Economic Geology of the University of Concepción for providing the facility to perform mineralogical analyses in the X-ray Laboratory.

Appendix A. Supporting information

Supplementary data associated with this article can be found in the online version at doi:10.1016/j.apcata.2025.120410.

Data Availability

Data will be made available on request.

References

[1] N.Ch Jana, S. Sethi, R. Saha, B. Bagh, Aerobic oxidation of vanillyl alcohol to vanillin catalyzed by air-stable and recyclable copper complex and TEMPO under base-free conditions, Green. Chem. 24 (2022) 2542–2556, https://doi.org/10.1039/D1GC04690J.

[2] S. Dong, H. Zhang, X. Du, T. Yao, Y. Shang, L. Jing, J. Hu, Further revealing reaction mechanism on the oxidation behavior of the lignin model molecules, Comput. Theor. Chem. 1230 (2023) 114382, https://doi.org/10.1016/j.comptc.2023.114382.

[3] R. Ghosh, S. Panda, A. MahaKhuda, R. Saha, B. Bagh, Base metal iron catalyzed sustainable oxidation of vanillyl alcohol to vanillic acid in deep eutectic solvents and implementation of vanillic acid for fine-chemical synthesis, RSC Sustain. 1 (2023) 1223–1232, https://doi.org/10.1039/D3SU00114H.

[4] Y. Kang, Z. Jin, J. Bian, X. Zhang, M. Jing, J. Wei, D. Fang, Non-hydroxyl radical dominated catalytic oxidation of lignin-derived vanillyl alcohol by H_2O_2 upon ionic liquids for vanillin production, in press, 2024, https://doi.org/10.1016/j.jiec.2024.07.024.

[5] A.C. Garade, N.S. Biradar, S.M. Joshi, V.S. Kshirsagar, R.K. Jha, C.V. Rode, Liquid phase oxidation of p-vanillyl alcohol over synthetic Co-saponite catalyst, Appl. Clay Sci. 53 (2011) 157–163, https://doi.org/10.1016/j.clay.2010.10.026.

[6] M.J. Beier, T.W. Hansen, J.-D. Grunwaldt, Selective liquid-phase oxidation of alcohols catalyzed by a silver-based catalyst promoted by the presence of ceria, J. Catal. 266 (2009) 320–330, https://doi.org/10.1016/j.jcat.2009.06.022.

[7] A. Kim, H.S. Bae, J.Ch Park, H. Song, K.H. Park, Surfactant-free Pd@pSiO_2 yolk–shell nanocatalysts for selective oxidation of primary alcohols to aldehydes, N. J. Chem. 39 (2015) 8153–8157, https://doi.org/10.1039/C5NJ01295C.

[8] W. Sun, S. Wu, Y. Lu, Y. Wang, Q. Cao, W. Fang, Effective control of particle size and electron density of Pd/C and Sn-Pd/C nanocatalysts for vanillin production via base-free oxidation, ACS Catal. 10 (14) (2020) 7699–7709, https://doi.org/10.1021/acscatal.0c01849.

[9] M. Melián-Rodríguez, S. Saravanamurugan, S. Kegnæs, A. Riisager, Aerobic oxidation of veratryl alcohol to veratraldehyde with heterogeneous ruthenium catalysts, Top. Catal. 58 (2015) 1036–1042, https://doi.org/10.1007/s11244-015-0472-z.

[10] D.V. Bavykin, A.A. Lapkin, P.K. Plucinski, J.M. Friedrich, F.C. Walsh, TiO_2 nanotube-supported ruthenium(III) hydrated oxide: a highly active catalyst for selective oxidation of alcohols by oxygen, J. Catal. 235 (2005) 10–17, https://doi.org/10.1016/j.jcat.2005.07.012.

[11] P. Lin, R. Shang, Q. Zhang, B. Gu, Q. Tang, F. Jing, Q. Cao, W. Fang, One-pot synthesis of finely-dispersed Au nanoparticles on ZnO hexagonal sheets for base-free aerobic oxidation of vanillyl alcohol, Catal. Sci. Technol. 12 (2022) 4613–4623, https://doi.org/10.1039/D2CY00837H.

[12] S. Rautiainen, J. Chen, M. Vehkamäki, T. Repo, Oxidation of vanillin with supported gold nanoparticles, Top. Catal. 59 (2016) 1138–1142, https://doi.org/10.1007/s11244-016-0633-8.

[13] A. Abad, P. Concepción, A. Corma, H. García, A collaborative effect between gold and a support induces the selective oxidation of alcohols, Angew. Chem. Int. Ed. 44 (2005) 4066–4069, https://doi.org/10.1002/anie.200500382.

[14] L. Yang, R. Ma, H. Zeng, Z. Rui, Yongdan Li, MOF-templated core-shell Co(II/III)@ZnO hexagonal prisms for selective oxidation of vanillyl alcohol, Catal. Today 355 (2020) 280–285, https://doi.org/10.1016/j.cattod.2019.02.031.

[15] J. Zakzeski, P.C.A. Bruijnincx, A.L. Jongerius, B.M. Weckhuysen, The catalytic valorization of lignin for the production of renewable chemicals, Chem. Rev. 110 (6) (2010) 3552–3599, https://doi.org/10.1021/cr900354u.

[16] M. Cui, L. Dong, Z. Shen, T. Guo, W. Zhao, Ch Liang, X. Liu, D. Wang, F. Wang, Z. Jiang, S. Fu, Preparation of porous carbon supported Co element doping spinel copper ferrite for the catalytic oxidation of vanillyl alcohol, Appl. Catal. A 664 (2023) 119325, https://doi.org/10.1016/j.apcata.2023.119325.

[17] N. Gayathri, P. Tamizhdurai, C. Kavitha, V.L. Mangesh, P. Santhana Krishnan, A. Vijayaraj, R. Kumaran, N.Siva Kumar, A.S. Al-Fatesh, S.B. Alreshaidan, Fe-Ni bimetallic supported on mordenite catalyst for selective oxidation of veratryl alcohol in a continuous reactor, Arab. J. Chem. 17 (2024) 105506, https://doi.org/10.1016/j.arabjc.2023.105506.

[18] V. Augugliaro, G. Camera-Roda, V. Loddo, G. Palmisano, L. Palmisano, F. Parrino, M.A. Puma, Synthesis of vanillin in water by TiO_2 photocatalysis, Appl. Catal. B 111–112 (2012) 555–561, https://doi.org/10.1016/j.apcatb.2011.11.007.

[19] M. Bellardita, M. Feilizadeh, R. Fiorenza, S. Scirè, L. Palmisano, V. Loddo, Selective aqueous oxidation of aromatic alcohols under solar light in the presence of TiO_2 modified with different metal species, Photochem. Photobiol. Sci. 21 (2022) 2139–2151, https://doi.org/10.1007/s43630-022-00284-2.

[20] A.Malek Djaballah, M. Bellardita, L. Palmisano, V. Loddo, M. Umair, C. M. Pecoraro, R. Bagtache, M. Trari, Facile preparation of $CuBi_2O_4/TiO_2$ heterosystems employed for simulated solar-light selective oxidation of 4-methoxybenzyl alcohol model compound, Mol. Catal. 546 (2023) 113251, https://doi.org/10.1016/j.mcat.2023.113251.

[21] P. Zhang, T. Wang, J. Gong, Mechanistic understanding of the plasmonic enhancement for solar water splitting, Adv. Mater. 27 (2015) 5328–5342, https://doi.org/10.1002/adma.201500888.

[22] G. Zheng, S. Mourdikoudis, Z. Zhang, Plasmonic metallic heteromeric nanostructures, Small 16 (2020) 2002588, https://doi.org/10.1002/smll.202002588.

[23] P. Han, W. Martens, E.R. Waclawik, S. Sarina, H. Zhu, Metal nanoparticle photocatalysts: synthesis, characterization, and application, Part. Part. Syst. Charact. 35 (2018) 1700489, https://doi.org/10.1002/ppsc.201700489.

[24] N.P. Radhika, R. Selvin, R. Kakkar, A. Umar, Recent advances in nano-photocatalysts for organic synthesis, Arab. J. Chem. 12 (2019) 4550–4578, https://doi.org/10.1016/j.arabjc.2016.07.007.

[25] T. Parangi, M.K. Mishra, Titania nanoparticles as modified photocatalysts: a review on design and development, Comments Inorg. Chem. 39 (2) (2019) 90–126, https://doi.org/10.1080/02603594.2019.1592751.

[26] H. Martínez Q, J.A. Neira, Á.A. Amaya, D. Blach V, C.H. Campos, F. Martínez, Selective oxidation of glycerol mediated by surface plasmon of gold nanoparticles deposited on titanium dioxide nanowires, Chemosphere 364 (2024) 142995, https://doi.org/10.1016/j.chemosphere.2024.142995.

[27] J.C. Scaiano, K.G. Stamplecoskie, G.L. Hallett-Tapley, Photochemical Norrish type I reaction as a tool for metal nanoparticle synthesis: importance of proton coupled electron transfer, Chem. Commun. 48 (2012) 4798–4808, https://doi.org/10.1039/C2CC30615H.

[28] A. Gellé, T. Jin, L. Garza, G.D. Price, L.V. Besteiro, A. Moores, Applications of Plasmon-Enhanced Nanocatalysis to Organic Transformations, 986–104, Chem. Rev. 120 (2020), https://doi.org/10.1021/acs.chemrev.9b00187.

[29] H. Tang, F. Liu, J. Wei, B. Qiao, K. Zhao, Y. Su, Ch Jin, L. Li, J. Liu, J. Wang, T. Zhang, Ultrastable Hydroxyapatite/Titanium-Dioxide-Supported Gold Nanocatalyst with Strong Metal–Support Interaction for Carbon Monoxide Oxidation, Angew. Chem. Int. Ed. 55 (2016) 10606, https://doi.org/10.1002/anie.201601823.

[30] K. Shanmugaraj, T.M. Bustamante, J.N. Díaz de León, Radhamanohar Aepuru, Ramalinga Viswanathan Mangalaraja, Cecilia C. Torres, Cristian H. Campos, Noble metal nanoparticles supported on titanate nanotubes as catalysts for selective hydrogenation of nitroarenes, Catal. Today 392–393 (2022) 93–104, https://doi.org/10.1016/j.cattod.2021.09.003.

[31] K. Shanmugaraj, R.V. Mangalaraja, C.H. Campos, D.P. Singh, R. Aepuru, A. Thirumurugan, M.A. Gracia-Pinilla, S. Shaji, Gold nanoparticles decorated two-dimensional TiO_2 nanosheets as effective catalyst for nitroarenes and rhodamine B dye reduction in batch and continuous flow methods, Inorg. Chem. Commun. 149 (2023) 110406, https://doi.org/10.1016/j.inoche.2023.110406.

[32] K. Shanmugaraj, S. Bedoya, D. González-Vera, R.V. Mangalaraja, S. Vigneshwaran, J.N.Díaz de León, C. Herrera, A.G. Al-Sehemi, C.H. Campos, Palladium nanoparticles immobilized on TiO_2 nanosheets matrix for the valorization of furfural to produce tetrahydrofurfuryl alcohol https://doi.org/10.1016/j.jece.2024.113442.

[33] V.C. Ferreira, M.R. Nunes, A.J. Silvestre, O.C. Monteiro, Synthesis and properties of Co-doped titanate nanotubes and their optical sensitization with methylene blue, Mater. Chem. Phys. 142 (2013) 355–362, https://doi.org/10.1016/j.matchemphys.2013.07.029.

[34] V.A. Sugiawati, F. Vacandio, A. Galeyeva, A.P. Kurbatov, T. Djenizian, Enhanced Electrochemical Performance of Electropolymerized Self-Organized TiO_2 Nanotubes Fabricated by Anodization of Ti Grid, Front. Phys. 7 (2019) 179, https://doi.org/10.3389/fphy.2019.00179.

[35] T. Gupta, Samriti, J. Cho, J. Prakash, Hydrothermal synthesis of TiO_2 nanorods: formation chemistry, growth mechanism, and tailoring of surface properties for photocatalytic activities, Mater. Chem. 20 (2021) 100428, https://doi.org/10.1016/j.mtchem.2021.100428.

[36] J. Dai, J. Yang, X. Wang, L. Zhang, Y. Li, Enhanced visible-light photocatalytic activity for selective oxidation of amines into imines over TiO_2(B)/anatase mixed-phase nanowires, Appl. Surf. Sci. 349 (2015) 343–352, https://doi.org/10.1016/j.apsusc.2015.04.232.

[37] C.C. Torres, V.A. Jiménez, C.H. Campos, J.B. Alderete, R. Dinamarca, T. M. Bustamante, B. Pawelec, Gold catalysts supported on TiO_2-nanotubes for the selective hydrogenation of p-substituted nitrobenzenes, Mol. Catal. 447 (2018) 21–27, https://doi.org/10.1016/j.mcat.2017.12.039.

[38] R. Yoshida, Y. Suzuki, S. Yoshikawa, Syntheses of TiO_2(B) nanowires and TiO_2 anatase nanowires by hydrothermal and post-heat treatments, J. Solid State Chem. 178 (2005) 2179–2185, https://doi.org/10.1016/j.jssc.2005.04.025.

[39] H.H. Kung, M.C. Kung, C.K. Costello, Supported Au catalysts for low temperature CO oxidation, J. Catal. 216 (2003) 425–432, https://doi.org/10.1016/S0021-9517(02)00111-2.

[40] Y. Suzuki, S. Pavasupree, S. Yoshikawa, R. Kawahata, Natural rutile-derived titanate nanofibers prepared by direct hydrothermal processing, J. Mater. Res. 20 (2005) 1063–1070, https://doi.org/10.1557/JMR.2005.0135.

[41] R. Yoshida, Y. Suzuki, S. Yoshikawa, Effects of synthetic conditions and heat-treatment on the structure of partially ion-exchanged titanate nanotubes, Mater. Chem. Phys. 91 (2005) 409–416, https://doi.org/10.1016/j.matchemphys.2004.12.010.

[42] K. Kordás, M. Mohl, Z. Kónya, Á. Kukovecz, Layered titanate nanostructures: perspectives for industrial exploitation, Transl. Mater. Res. 2 (2015) 015003, https://doi.org/10.1088/2053-1613/2/1/015003.

[43] P. Dong, B. Liu, Y. Wang, L. Guo, Y. Huang, S. Yin, A Study on the $H_2Ti_3O_7$ sheet-like products during the formation process of titanate nanotubes, J. Electrochem. Soc. 158 (2011) K183, https://doi.org/10.1149/1.3610406.

[44] M. Thommes, K. Kaneko, A.V. Neimark, J.P. Olivier, F. Rodriguez-Reinoso, J. Rouquerol, K.S.W. Sing, Physisorption of gases, with special reference to the evaluation of surface area and pore size distribution (IUPAC Technical Report), Pure Appl. Chem. 87 (9-10) (2015) 1051–1069, https://doi.org/10.1515/pac-2014-1117.

[45] Ch Ban, B. Li, J. Ma, Y. Feng, Y. Ch. Lin, Y. Chen, Y. Wang, K. Duan, L. Zhou, S. Gan, X. Wang, Zhou, Plasmonic Au–TiO_2 interactions for augmented photocatalytic hydrogen evolution, Ceram. Int. 50 (2024) 15444–15451, https://doi.org/10.1016/j.ceramint.2024.02.020.

[46] A. Das, P. Dagar, S. Kumar, A. Kumar Ganguli, Effect of Au nanoparticle loading on the photo-electrochemical response of Au–P25–TiO_2 catalysts, J. Solid State Chem. 281 (2020) 121051, https://doi.org/10.1016/j.jssc.2019.121051.

[47] Y. Yu, W. Wen, X.-Y. Qian, J.-B. Liu, J.-M. Wu, UV and visible light photocatalytic activity of Au/TiO_2 nanoforests with Anatase/Rutile phase junctions and controlled Au locations, Sci. Rep. 7 (2017) 41253, https://doi.org/10.1038/srep41253.

[48] S.-W. Lai, J.-W. Park, S.-H. Yoo, J.-M. Ha, E.-H. Song, S.-O. Cho, Surface synergism of Pd/$H_2Ti_3O_7$ composite nanowires for catalytic and photocatalytic hydrogen production from ammonia borane, Int. J. Hydrog. Energy 41 (2016) 3428–3435, https://doi.org/10.1016/j.ijhydene.2015.12.058.

[49] A.G. Dosado, W.-T. Chen, A. Chan, D. Sun-Waterhouse, G.I.N. Waterhouse, Novel Au/TiO_2 photocatalysts for hydrogen production in alcohol–water mixtures based on hydrogen titanate nanotube precursors, J. Catal. 330 (2015) 238–254, https://doi.org/10.1016/j.jcat.2015.07.014.

[50] X. Zhang, W. Zhang, Y. Xu, M. Jin, Defective Titanium Dioxide-supported Ultrasmall Au Clusters for Photocatalytic Hydrogen Production, Front. Phys. 8 (2020), https://doi.org/10.3389/fphy.2020.616349.

[51] G. Yu, B. Tang, Q. Luo, H. Chen, Z. Yin, Z. Zhang, Z. Wang, B. Lv, S. Shan, Hydrogel microspheres supported TiO_2 loaded with Au nanoparticles as a novel photocatalyst for solar-to-hydrogen conversion, Int. J. Hydrog. Energy 78 (2024) 236–243, https://doi.org/10.1016/j.ijhydene.2024.06.218.

[52] C. Wan, L. Zhou, L. Sun, L. Xu, D. Cheng, F. Chen, X. Zhan, Y. Yang, Boosting visible-light-driven hydrogen evolution from formic acid over AgPd/2D g-C_3N_4 nanosheets Mott-Schottky photocatalyst, Chem. Eng. J. 396 (2020) 125229, https://doi.org/10.1016/j.cej.2020.125229.

[53] A. Wang, S. Wu, J. Dong, R. Wang, J. Wang, J. Zhang, S. Zhong, S. Bai, Interfacial facet engineering on the Schottky barrier between plasmonic Au and TiO_2 in boosting the photocatalytic CO_2 reduction under ultraviolet and visible light irradiation, Chem. Eng. J. 404 (2021) 127145, https://doi.org/10.1016/j.cej.2020.127145.

[54] R.J. Wong, J. Scott, G.K.-C. Low, H. Feng, Y. Du, J.N. Hart, R. Amal, Investigating the effect of UV light pre-treatment on the oxygen activation capacity of Au/TiO_2, Catal. Sci. Technol. 6 (2016) 8188–8199, https://doi.org/10.1039/C6CY01717G.

[55] H. Martínez, J. Neira, Á.A. Amaya, E.A. Páez-Mozo, F. Martínez Ortega, Selective Photooxidation of Valencene and Thymol with Nano-TiO_2 and O_2 as Oxidant, Molecules 28 (9) (2023) 3868, https://doi.org/10.3390/molecules28093868.

[56] H. Chen, G. Liu, L. Wang, Switched photocurrent direction in Au/TiO_2 bilayer thin films, Sci. Rep. 5 (2015) 10852, https://doi.org/10.1038/srep10852.

[57] G. Žerjav, J. Zavašnik, J. Kovač, A. Pintar, The influence of Schottky barrier height onto visible-light triggered photocatalytic activity of TiO_2 + Au composites, Appl. Surf. Sci. 543 (2021) 148799, https://doi.org/10.1016/j.apsusc.2020.148799.

[58] A. Nikolskaia, M. Vildanova, S. Kozlov, N. Tsvetkov, L. Larina, O. Shevaleevskiy, Charge Transfer in Mixed-Phase TiO_2 Photoelectrodes for Perovskite Solar Cells, Sustainability 12 (3) (2020) 788, https://doi.org/10.3390/su12030788.

[59] G. Panomsuwan, S. Wongcharoen, Ch Chokradcharoen, M. Tipplook, O. Jongprateep, N. Saito, Au nanoparticle-decorated TiO_2 hollow fibers with enhanced visible-light photocatalytic activity toward dye degradation, RSC Adv. 12 (2022) 193–200, https://doi.org/10.1039/D1RA07323K.

[60] H. Zhou, B. Li, J. Liu, W. Yang, W. Wang, X. Hu, S. Wang, Construction of novel tandem reaction system coupling H_2O_2 production with in situ bleaching over Au/TiO_2 photocatalyst with different metal-support interactions, Process Saf. Environ. Prot. 183 (2024) 355–364, https://doi.org/10.1016/j.psep.2023.12.061.

[61] D. Yu, P. Lei, Y. Li, W. Shen, M. Zhong, J. Zhang, S. Guo, Catalytic Oxidation of Veratryl Alcohol Derivatives Using RuCo/rGO Composites, Chem. Eur. J. 28 (2022) e202104380, https://doi.org/10.1002/chem.202104380.

[62] N. Serpone, Relative photonic efficiencies and quantum yields in heterogeneous photocatalysis, J. Photochem. Photobiol. A 104 (1997) 1–12, https://doi.org/10.1016/S1010-6030(96)04538-8.

[63] J. Szychliński, P. Bilski, K. Martuszewski, J. Blażejowski, Complementary Study on the Use of the Potassium Reinecke's Salt as a Chemical Actinometer, Analyst 114 (1989) 739–741, https://doi.org/10.1039/AN9891400739.

[64] A. Mahdavi-Shakib, J. Sempel, L. Babb, A. Oza, M. Hoffman, T.N. Whittaker, B. D. Chandler, R.N. Austin, Combining Benzyl Alcohol Oxidation Saturation Kinetics and Hammett Studies as Mechanistic Tools for Examining Supported Metal Catalysts, ACS Catal. 10 (2020) 10207–10215, https://doi.org/10.1021/acscatal.0c02212.

[65] A. Abad, A. Corma, H. García, Catalyst Parameters Determining Activity and Selectivity of Supported Gold Nanoparticles for the Aerobic Oxidation of Alcohols: The Molecular Reaction Mechanism, Chem. Eur. J. 14 (2008) 212–222, https://doi.org/10.1002/chem.200701263.

[66] P. Fristrup, L.B. Johansen, C.H. Christensen, Mechanistic Investigation of the Gold-catalyzed Aerobic Oxidation of Alcohols, Catal. Lett. 120 (2008) 184–190, https://doi.org/10.1007/s10562-007-9301-8.

[67] G. Kumar, L. Tibbitts, J. Newell, B. Panthi, A. Mukhopadhyay, R.M. Rioux, C. J. Pursell, M. Janik, B.D. Chandler, Evaluating differences in the active-site electronics of supported Au nanoparticle catalysts using Hammett and DFT studies, Nat. Chem. 10 (2018) 268–274, https://doi.org/10.1038/nchem.2911.

[68] A. Kumar, K. Kumar, V. Krishnan, Sunlight driven methanol oxidation by anisotropic plasmonic Au nanostructures supported on amorphous titania: Influence of morphology on photocatalytic activity, Mater. Lett. 245 (2019) 45–48, https://doi.org/10.1016/j.matlet.2019.02.091.

[69] R. Behling, G. Chatel, S. Valange, Sonochemical oxidation of vanillyl alcohol to vanillin in the presence of a cobalt oxide catalyst under mild conditions, Ultrason. Sonochem. 36 (2017) 27–35, https://doi.org/10.1016/j.ultsonch.2016.11.015.

[70] L. Zhao, B. Zhang, X. Xiao, F.Long Gu, R.-Q. Zhang, Roles of the active species involved in the photocatalytic oxidation of benzyl alcohol into benzaldehyde on TiO_2 under UV light: Experimental and DFT studies, J. Mol. Catal. A 420 (2016) 82–87, https://doi.org/10.1016/j.molcata.2016.03.012.

[71] O. Al-Madanat, B.Nascimento Nunes, Y. AlSalka, A. Hakki, M. Curti, A.O. T. Patrocinio, D.W. Bahnemann, Application of EPR Spectroscopy in TiO_2 and Nb_2O_5 Photocatalysis, Catalysts 11 (2021) 1514, https://doi.org/10.3390/catal11121514.

[72] J.B. Priebe, M. Karnahl, H. Junge, M. Beller, D. Hollmann, A. Brückner, Water reduction with visible light: synergy between optical transitions and electron transfer in Au-TiO_2 catalysts visualized by insitu EPR spectroscopy, Angew. Chem. Int. Ed. 52 (2013) 11420–11424, https://doi.org/10.1002/anie.201306504.

[73] J. Nie, J. Schneider, F. Sieland, L. Zhou, S. Xia, D.W. Bahnemann, New insights into the surface plasmon resonance (SPR) driven photocatalytic H_2 production of Au–TiO_2, RSC Adv. 8 (2018) 25881–25887, https://doi.org/10.1039/C8RA05450A.

[74] Y.O. Ibrahim, A. Hezam, T.F. Qahtan, A.H. Al-Aswad, M.A. Gondal, Q.A. Drmosh, Laser-assisted synthesis of Z-scheme TiO_2/rGO/g-C_3N_4 nanocomposites for highly enhanced photocatalytic hydrogen evolution, Appl. Surf. Sci. 534 (2020) 147578, https://doi.org/10.1016/j.apsusc.2020.147578.

[75] L. Zhao, F.Long Gu, M. Kim, M. Miao, R.-Q. Zhang, DFT study of benzyl alcohol/TiO_2 interfacial surface complex: reaction pathway and mechanism of visible light absorption, J. Mol. Model 23 (2017) 285, https://doi.org/10.1007/s00894-017-3451-4.

[76] D.A. Giannakoudakis, A. Qayyum, M. Barczak, R.F. Colmenares-Quintero, P. Borowski, K. Triantafyllidis, J.C. Colmenares, Mechanistic and kinetic studies of benzyl alcohol photocatalytic oxidation by nanostructured titanium (hydro)oxides: do we know the entire story? Appl. Catal. B 320 (2023) 121939 https://doi.org/10.1016/j.apcatb.2022.121939.

[77] S. Higashimoto, R. Shirai, Y. Osano, M. Azuma, H. Ohue, Y. Sakata, H. Kobayashi, Influence of metal ions on the photocatalytic activity: Selective oxidation of benzyl alcohol on iron (III) ion-modified TiO_2 using visible light, J. Catal. 311 (2014) 137–143, https://doi.org/10.1016/j.jcat.2013.11.013.

[78] H. Kobayashi, S. Higashimoto, DFT study on the reaction mechanisms behind the catalytic oxidation of benzyl alcohol into benzaldehyde by O_2 over anatase TiO_2 surfaces with hydroxyl groups: Role of visible-light irradiation, Appl. Catal. B 170–171 (2015) 135–143, https://doi.org/10.1016/j.apcatb.2015.01.035.

[79] P.D. Giorgi, N. Elizarov, S. Antoniotti, Selective oxidation of activated alcohols by supported gold nanoparticles under an atmospheric pressure of O_2: batch and continuous-flow studies, ChemCatChem 9 (2017) 1830–1836, https://doi.org/10.1002/cctc.201700179.

[80] B. Zhao, R.J. Kashtiban, S. Huband, M. Walker, R.I. Walton, Cerium-Organic Framework UiO-66(Ce) as a support for nanoparticulate gold for use in oxidation catalysis, Chem. Asian J. 19 (2024) e202401035, https://doi.org/10.1002/asia.202401035.

[81] C.S. Hinde, D. Ansovini, P.P. Wells, G. Collins, S.Van Aswegen, J.D. Holmes, T.S. A. Hor, R. Raja, Elucidating structure−property relationships in the design of metalnanoparticle catalysts for the activation of molecular oxygen, 5, ACS Catal. 5 (2015) 3807–3816, https://doi.org/10.1021/acscatal.5b00481.

[82] W. Zhang, Z. Xiao, J. Wang, W. Fu, R. Tan, D. Yin, Selective aerobic oxidation of alcohols over gold-palladium alloy catalysts using air at atmospheric pressure in water, ChemCatChem 11 (2019) 1779–1788, https://doi.org/10.1002/cctc.201900015.

[83] M. Wu, J.-H. Pang, P.-P. Song, J.-J. Peng, F. Xu, Q. Li, X.-M. Zhang, Visible light-driven oxidation of vanillyl alcohol in air with Au–Pd bimetallic nanoparticles on phosphorylated hydrotalcite, N. J. Chem. 43 (2019) 1964–1971, https://doi.org/10.1039/C8NJ05477K.